Effect of Disturbance and Water-induced Compaction on Void Ratio and Pre-consolidation Stress of Glacial Till

Master thesis

of

Satyanarayana Narra

Matriculation Number 2211120

Supervised

by

Prof. Dr. Dr. h. c. Reinhard F. Hüttl

Chair of Soil Protection and Recultivation

Dr. rer. nat. Oliver stock

Chair of Soil Protection and Recultivation

realised and written

at the Chair of Soil Protection and Recultivation,

Faculty of Environmental Sciences and Process Engineering,

Brandenburg University of Technology Cottbus, Germany

12th of September 2005

Einfluss von Lockerung und wasserinduzierter Verdichtung auf die Porenziffer und die Vorbelastung von Geschiebemergel

Master Arbeit

of

Satyanarayana Narra

Matriculation Number 2211120

Betreuer

Prof. Dr. Dr. h. c. Reinhard F. Hüttl

Lehrstuhl für Bodenschutz und Rekultivierung

Dr. rer. nat. Oliver stock

Lehrstuhl für Bodenschutz und Rekultivierung

Der Fakultät für Umweltwissenschaften und verfahrenstechnik

der Brandenburgische Technische Universität Cottbus Vorgelegte Dissertation

zur Erlangung des akademischen Grades eines

12th of September 2005

Declaration

I hereby declare that the submitted thesis work has been completed by me and that I have not used any other than permitted reference sources or materials. All references and other sources used by me have been appropriately acknowledged in this work. I further declare that this work has not been submitted for the purpose of academic examination, either in its original or similar form, anywhere else.

Versicherung

Ich versichere, dass ich diese Arbeit selbständig verfasst und keine anderen als die angegebenen Hilfsmittel benutzt habe. Die den benutzten Hilfsmitteln wÖrtlich oder inhaltlich entnommenen stellen habe ich unter Quellenangaben kenntlich gemacht. Die Arbeit hat in gleicher oder ähnlicher Form noch keiner anderen Prüfungsbehörde vorgelegen.

Declared in Cottbus, September 2005

Narra Satyanarayana

Acknowledgements

This master thesis was realised and written from May. 2005 till August 2005 at the Chair of Soil Protection and Recultivation, Faculty 4, Environmental and Resource Management in Brandenburg University of Technology, Cottbus, Germany.

I thank Prof. Dr. Dr. h.c. R. F. Hüttl, Chair of Soil Protection and Recultivation for accepting me to pursue my master thesis and I also like to extend my thanks to Dr. Oliver Stock, for providing me professional guidance and assistance at each and every step to accomplish my master thesis.

I like to acknowledge the members working at the Chair of Soil Protection and Recultivation and also the members from Soil mechanics department for helping me in the laboratory. I also extend my thanks for providing the laboratory facilities.

I would like to thank Mr. Christoph Helbach Dipl.-Ing. agr., for giving me assistance in sampling at the study site.

Last but not least, I like to thank Vattenfall Europe Mining AG in Cottbus for granting the permission to take samples from the study site.

Abstract

Soils deposited can undergo a sudden change in the structure when they are inundated with water resulting decrease in the volume. This process is known as water induced compaction. The decrease in volume occurs without any change in external loads and is only caused by the water, which results in the settlement of soil surface having a resultant potential to damage the structures. The water induced compaction process is characterized by sudden change in the voids or pores of the soil that are loaded at their natural water content and flooded. The objective of this thesis work was to understand the water induced consolidation process at agriculturally used reclaimed soils. The approach was to reproduce the situation occurring when the soil was subjected to water induced compaction at defined loads typical in the top soil (0 kPa to 20 kPa).

The glacial till used for the experiments was sampled in the Lusatian lignite-mining district located about 100 km southeast of Berlin, Germany. Sediment samples for different investigations were taken from the pre-cut section at 1500 m west of the eastern end from 3 m depth till 10 m depth. The glacial till used for the experiments derived from the sediment layer of Warthe sub-stage of the saalian glaciation. To characterize the soil properties at the pre-cut section, parameters like grain size distribution, soil bulk density, calcium carbonate content ($CaCo_3$) and water retention characteristics were measured.

The stability of the glacial till was evaluated using parameter pre-consolidation load. This was done in three sub-steps. The first step was determination of the stress-strain behaviour under natural conditions. In the second step the stress-strain behaviour of disturbed dry samples was simulated, which would be the situation in summer when the glacial till dries during transport. In the third step we saturated the disturbed dry samples which were subjected to different pre-loads to simulate the effect of saturation and re-compaction by precipitation. This work was exemplarily done for undisturbed samples and also for disturbed dry samples from 4 depths (4 m, 6 m, 8 m, and 10 m). Disturbed dry and saturated conditions were tested for samples from depths 4 m and 8 m.

i) It was found from the grain size distribution that the soil profile is uniformly distributed with different particle sizes. High soil bulk density was recorded, which were in the range of 1.9 g cm^{-3} to 2.0 g cm^{-3}. We observed that the carbonate content increased with the depths, in our observation it increased up to 5.4 %. From the water retention characteristics we observe that the samples from 4 m and 10 m depth do not have coarse pores where as 6 m and 8 m depth samples have coarse pores.

ii) We observed that the undisturbed samples showed a flat curve having the initial void ratio and final void ratio values within a small range (between 0.2 and 0.4), where as the disturbed dry and the disturbed saturated curves showed a huge difference in the initial and final void ratio values. The difference was decreasing with the increase in pre-loads. We found that pre-consolidation stress values obtained were not increasing with the increase in depth. We also observed a huge difference in the void ratio value of the disturbed dry and disturbed saturated curves and this difference was increasing with the increase in applied pre-loads. The disturbed saturated samples from the 4 m depth showed over-estimation of the results, where as the disturbed saturated samples from 8 m appeared to be realistic.

We found that the magnitude of water induced compaction increased with the increase in pre-loads and a decrease with respect to the depths.

Index of figures

Index of tables

Symbols and Abbreviations

a	Bailey emperical parameter
α	van-Genuchten-Parameter
b	Bailey emperical parameter
c	Bailey emperical parameter
exp	exponential constant (e = 2.72)
ε / e	Void ratio
ε_{min} / e_{min}	Final (Minimum) void ratio
ε_{max} / e_o / e_{max}	Initial (Maximum) void ratio
θ	Water content
θ_s	Saturated water content
θ_r	Residual water content
σ / σ_v	Applied stress
σ_{vmin}	Minimum applied stress
σ_{vmax}	Maximum applied stress
ρ_{soil} / ρ_o	Soil bulk density
$\rho_{particle}$ / ρ_m	Soil particle density
hPa	Hecto Pascal
k	Assouline empirical fitting parameter
kPa	Kilo Pascal
n	van-Genuchten-parameter
OCR	Over consolidation ratio
ω	Assouline empirical fitting parameter
P'_c / P	Pre-consolidation stress
P_o	Over-burden stress
pF	Logarithmic water tension

r_{min}	Radius of minimum curvature
R	Regression coefficient
RCL	Re-compression line / Regression line
S	Sand proportion
T	Clay proportion
U	Silt Proportion
VCL	Virgin compression line
°C	Degree Celsius

1. Introduction

1.1 Background

Since the early 1990's, in the Lower Lusatian lignite-mining district glacial till is used to restore arable land, which has been destroyed due to large-scale lignite mining operations. The glacial till in its natural state before excavation is highly compacted and shows a dense structure, bulk densities observed were in between 1.9 g cm^{-3} and 2.1 g cm^{-3}. The excavation process as an important step of the lignite mining operation causes the discontinuation of the glacial till. On the conveyor belt being another step in this operation, bulk density values got reduced and were in the range of 1.1-1.4 g cm^{-3} (Stock *et al.,* 2004). After dumping, bulk density values of the respective substrates increased within a short period up to a value of 1.8 g cm^{-3}. This increase was observed regardless, whether these substrates were used for agriculture or for nature protection purposes. As the latter land use is not combined with intensive soil treatment this finding indicates that high bulk density values of reclaimed soils are at least under the described conditions primarily 'a result of reconsolidation'. Hence, with regard to the test conditions, agricultural land use practices expose only a secondary impact on soil bulk density.

Investigations on meta-stable arrangements of particles, e.g. by Hartmann *et al.* (2002), point up that loose arrangements of particles, as it is created by tillage operations, or in this case by mining operation steps like excavation, transport and dumping, are unstable. If wetted, it tends to compact rapidly associated with negative effects on root development of crops (Lesturgez *et al.*, 2004). The phenomenon is also well known from the behaviour of loess soils in Lybia (Assallay *et al.*, 1996, 1997) and furthermore reported for agriculturally used soils in Germany by Horn and Rosteck (2000). This water-induced compaction phenomenon describes the increase of bulk density without additional loads, i.e. only by the weight of the soil itself, when the soil or the particle arrangement is wetted.

The process behind the phenomenon is that the additional water modifies the stress situation between the soil particles. Associated with the saturation, the equilibrium of the inner forces of the soil becomes unstable and is shifted to a new one. Since the stability of the soil matrix is a function of the number of contact points of the soil particles and the stress resistance between them, it means, that with the reduction of the stress resistance the number of contact points must increase to reach a new stable equilibrium. The result is that the soil compacts until this equilibrium is reached. After this the soil has reached a stable state.

Contrary to mechanical compaction, e.g. by high axial loads of agricultural equipment, where the compaction remains for small parts reversible, i.e. it is an elastic deformation, compaction by water-induced compaction is non-reversible, i.e. in this case it is almost a complete plastic deformation. As a consequence of this, Stock (2005) discussed the possibility to model the new equilibrium of inner strength exemplary for field samples from an agriculturally used post-mining site of the Lower Lusatian lignite mining district. The recent thesis will continue the approach of modelling of the inner strength, with the advantage that disturbed samples of glacial till were subjected to defined pre-consolidation loads to prove, if the modelling can reproduce the formerly stress. Additionally, changes of the inner strength were investigated displaying the situation of the glacial till before, during and after mining operation occurred.

1.2 Problem

Water-induced compaction is classically a phenomenon of loess soils, and it is usually studied within the context of soil mechanics and engineering geology (Bryant, 1989; Franzmeier *et al.*, 1989; Rogers *et al.*, 1994; Assallay et al., 1996, 1997). When loess soils are loaded and wetted the structure tends to collapse, i.e. water-induced compaction (hydro-consolidation) occurs and subsidence is caused (Figure 1). This can be considered as one of the major factors in causing damage to the buildings and other structures. Water-induced compaction is characterized by abrupt changes in the voids ratio 'ε' which describes the ratio of soil bulk density to the particle density minus one (Equation 5). The intensity of the collapse behaviour depends strongly on the clay content (Assallay *et al.,* 1998). Even though water-induced compaction is often reported from loess soil, Horn and Rosteck (2002), Hartmann *et al.* (2002) and Lesturgez *et al.* (2004) have shown that it is also common in sandy soils.

Due to the necessity to understand the water-induced compaction process consolidation tests were carried out on natural soils and artificial substrates. The approach of these tests was to reproduce the situation occurring when the soils show water-induced compaction behaviour. The tests consisted of the determination of the dry and saturated consolidation curve of the used soil and the substrate, respectively, and then a certain number of combined consolidation tests were carried out. The combined consolidation tests comprised the following steps: (i) loading the dry sample to a certain load, (ii) flooding the sample at this load level, (iii) the samples were drained to pF1.8 and the saturated samples were loaded stepwise from 0 to 2500 kPa to the maximum stress value.

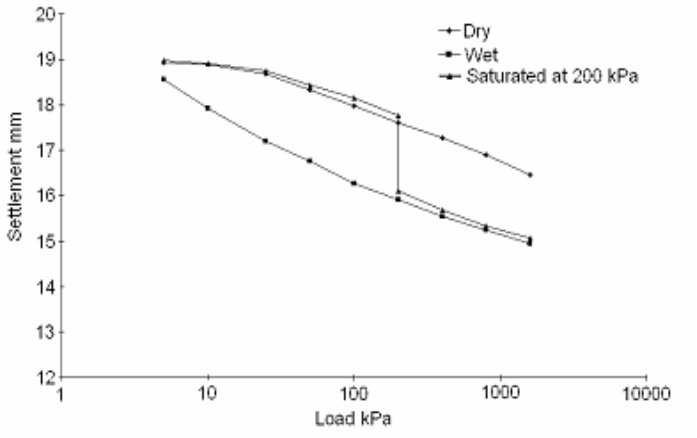

Figure 1. Hydro-compaction behaviour in loess soil (Miller et al., 1998). Two main curves are observed one for unsaturated behaviour and one for saturated behaviour. The third curve shows the characteristic collapse behaviour when the soil was saturated at 200kPa.

Stock *et al.* (2005) proposed an approach to predict the internal stress after water-induced compaction. He stated that in case of hydro-consolidation no elastic uplift occurs if the soil is discharged, due to the fact that deformation is exclusively plastic (Lesturgez, 2005). Vice versa means that, if the stress applied by stepwise reloading on a discharged soil sample is smaller than the stress applied by the soil column during hydro-consolidation no compaction occurs. A compaction occurs first, when the internal stress equilibrium is exceeded. On the basis of this theory, it should be shown that the point of interception between consolidation curve and effective void ratio threshold represents the effective stress acting in a soil specimen at a certain depth defined by the weight of the wetted soil column above (Figure 2).

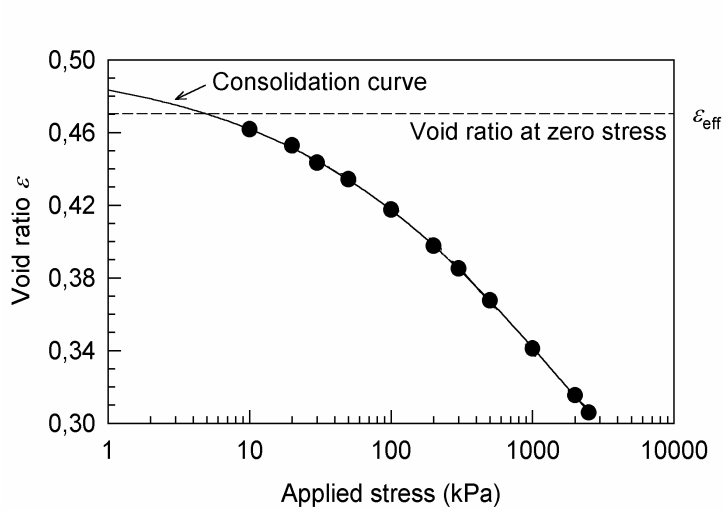

Figure 2. Modelling internal stress of a glacial till specimen from a post-mining reclamation site (after Stock (2005). Effective stress is at the point where the curve meets the maximum void ratio value

This approach shows that the soil deformation is associated with the water-induced compaction and it also gives a possibility to predict the stress acting in a soil specimen caused by water-induced compaction. The recent work picks this approach up with the advantage that specimens of glacial till were subjected to specific loads representing the internal stress of specific soil depths.

1.3 Goals and Questions

The goal of the recent work is to prove the approach to predict the internal stress after water-induced compaction (hydro-consolidation) on the basis of consolidation tests with disturbed glacial till samples, which were formerly subjected to defined stress values representing defined depths of the soil. Further, consolidation tests with undisturbed wet and disturbed dry samples should prove the changes in the internal stress due to mining operations.

With respect to the goals following questions should be answered:

- Will there be an increase in pre-consolidation load with respect to the depths at pre-cut section / under natural conditions?
- What would be the effect of water induced compaction on void ratios in disturbed samples taken from different depths with different pre-loads?
- Will the estimated pre-consolidation stress (applied load) be equal to the calculated values from the graph?

1.4 Structure of the thesis

This thesis work is dissected in 3 parts

1) Characteristic properties of glacial till layer were investigated with respect to the changes with in soil profile with depths such as a) Bulk density and Carbonate content, b) Grain size distribution, and c) pF-curve determination. The Basis for the discussion will be on impact of the soil column height on internal stress (pre-consolidation stress) or impact of $CaCo_3$ on stress strain behaviour of the samples. Grain size distribution was used to know the distribution of the soil particles in the glacial till which showed that the particles were homogenously distributed. The water retention curve (pF-curve) is one of the hydraulic characteristics of the soil. The water retention curve illustrates the dependency of the water content of the soil and the presence of coarse pores if any in the glacial till.

2) The samples were treated in three different steps:

In step 1 the stress-strain behaviour under undisturbed conditions was investigated where the Samples are directly taken from the field and were placed on the suction plates at a tension of 63.1 hPa. This is useful in simulating the natural conditions of soil profile.

In step 2 the Stress-strain behaviour under disturbed conditions was investigated, for this disturbed dry samples were used, which are useful in simulating the situation when groundwater levels drop, the upper layer of newly dry soil no longer has a column of water to help support it. As a result, the soil may become compressed under its own increased weight.

In the third step, disturbed dry samples from different depths were saturated with different pre-loads (0 kPa, 5 kPa, 10 kPa, 20 kPa) on the suction plate at a water tension of 63.1 hPa (pF1.8). This is helpful in simulating the field conditions when the water level has increased and the non-stable equilibrium of internal stress is shifted to a new equilibrium.

3) Pre-consolidation stress: we tried to check whether the estimated pre-consolidation stress using the soil bulk density was equal to that of the calculated pre-consolidation stress using Casagrande graphical method under natural conditions, where as in the case of disturbed samples the estimated stress was the applied pre-load. Pre-consolidation stress was derived from the compressive behaviour of soil, which is expressed graphically in the relationship between the logarithm of applied stress, $\log(\sigma)$, and void ratio, ε.

2. State of Knowledge

2.1 Stress-strain behaviour

Figure 3 shows the stress-strain behaviour curve with the rebound at a certain stress. The value of maximum void ratio is measures at the zero stress represented by e_{max}. Virgin compression line is the line drawn tangential to the curve, which is represented as VCL. When the stress is applied on the soil samples the value of the void ratio gradually decreases which is till the point of maximum curvature where the value of pre-consolidation stress is determined. Beyond this point the curve shows a steeper gradient, which is due to the reason that the soil sample is completely in plastic stage. When the stress is unloaded or removed at point 1, the curve shows a rebound and when again the stresses are added the plastic region is reached at point 2 instead of point 1 and follows the path of VCL.

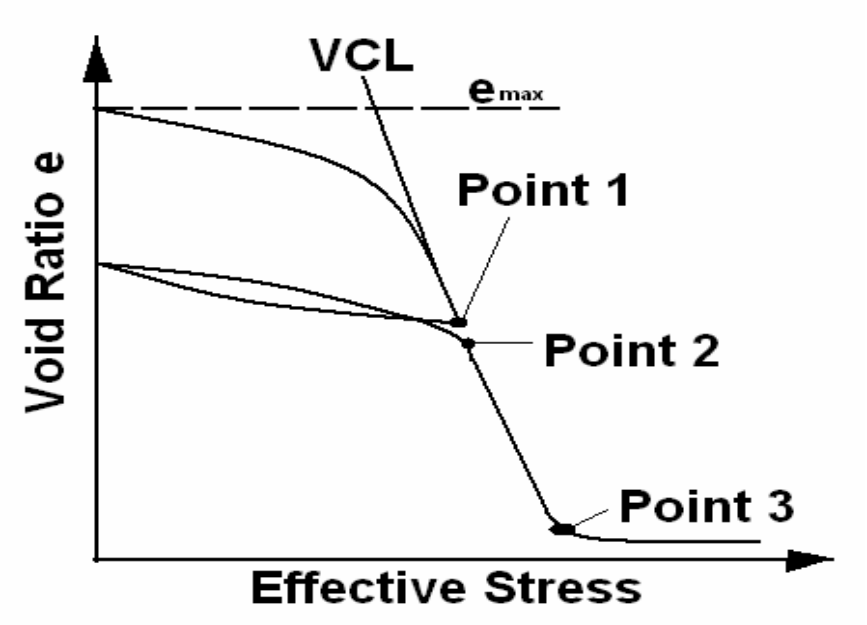

Figure 3. Curve showing the stress-strain behaviour with the rebound at a certain stress

From Figure 3 we can also observe that the value of the minimum (final) void ratio obtained at the highest stress applied cannot be less then or equal to zero, where as the value of maximum soil bulk density cannot be more then 2.65 g cm^{-3} (Bodman *et al.,* 1965). This is shown in Figure 3 which represents the curve after point 3, which can be due to the reason that the soil particles are ideally packed and cannot undergo any compression further. The highest bulk densities were recorded with the mixtures of loamy sand textures.

Badawy (2004) has shown that there will be a change from elastic to plastic behavior with the increase in soil water content, due to the lubrication effect of water, which disrupts the inter particle frictional forces at points of contact. The soils packed under dry condition will have higher pre-consolidation stress values, where as if the soil has water content (generally pF1.8) the internal forces between the particles increase due to adhesion. With the increase in water content during compaction the void ratio decreases to minimum and then increases (Bodman *et al.,* 1965). The grain size distribution also affects the consolidation process. If the soil is well graded with all the sizes of soil particles the compression will be lesser as the void spaces between the soil particles will be filled by the smaller particles and reach ideally packed situation. The soils with different grain size distribution, the arrangement will be different. The soil compression also depends on the shape of the soil particles, if the soil particles are round (ideal shape) they will not undergo compression.

2.2 Water-induced compaction

Deposits that undergo a sudden change in structural configuration when inundated with water accompanying a decrease in volume. This process is also known as water-induced compaction, hydro-compaction, hydro-consolidation, collapse etc. Soils prone to collapse include low density, porous sands and silts deposited. The volume change occurs with no change in external load, caused solely by the effect of water. The effect of soil compression or collapse is settlement of the ground surface with a resultant potential to damage foundations of structures and other improvements. Hydro-consolidation is a term descriptive of the relatively rapid settlement of certain soils upon saturation. Hydro-collapse of loess continues to cause major geotechnical problems over the world. Hydro-consolidation has been described worldwide in the context of Fragipan formation (Bryant, 1989). Hydro-consolidation has been also described by Lesturgez (2005) for sandy soils in Thailand, However similar processes have been described under the term slumping and re-compaction in the context of hard setting soils (Mullins *et al.,* 1990)and tilled layers of arable soils (Hartmann *et al.*, 2002).

Soil collapse, or hydro-consolidation, occurs when soils undergo a rearrangement of their grains due to a loss of cohesion or cementation, resulting in substantial and rapid settlement even under relatively low loads. This phenomenon typically occurs in recently deposited soils in an arid or semi-arid environment. Wind-deposited sands and silts deposited during flash floods are particularly susceptible to hydro-consolidation. Man-made fills, which are loose and unconsolidated, may also be subject to collapse.

When these soils are saturated from irrigation water or a rise in the groundwater table, pores and voids between the soil particles are removed, and the soils collapse. Water saturation affects the stress equilibrium between the grains causing collapse settlement, known technically, as hydro-consolidation. Fill placed in a relatively dry state, as is often the case with shaley or rocky mine spoils, inducing post-construction settlement likely to consist more of the collapse variety. Fill placed wet will undergo less collapse.

Hydro-consolidation has been intensively investigated under laboratory conditions by Assalay *et al.* (1998) and Lesturgez (2005). Both demonstrated that starting from dry compaction the water induced collapse is a single event, resulting with additional consolidation, thus causing a new arrangement of particles that fill up the space and eliminate all voids larger then the particles. This close packing reduces porosity, restricts water and air circulation, and usually inhibits root penetration (Constantini, 2004).

Figure 4 shows the dry and wet curves of the soil. We observe that the collapse has occurred, when the sample was wetted at a certain stress. This explains the hydro-consolidation. Hydro-consolidation, occurs when soils undergo a rearrangement of their grains, which result in a sudden settlement even under low stresses. This indicates the situation when the soils will be saturated by rise in the groundwater, the forces between the soil particles will be reduced, and the soil collapse will occur. The process of the soil collapse is essentially a transition from the open particle packing stage to a closer particle packing stage. The magnitude of the collapse can be measure by the difference in the void ratio values. Lesturgez *et al.* (2004) showed that the collapse will not occur at very high stresses. Assalay *et al.* (1998) has also shown that the progressive densification of the soil occurs under increasing overburden stress.

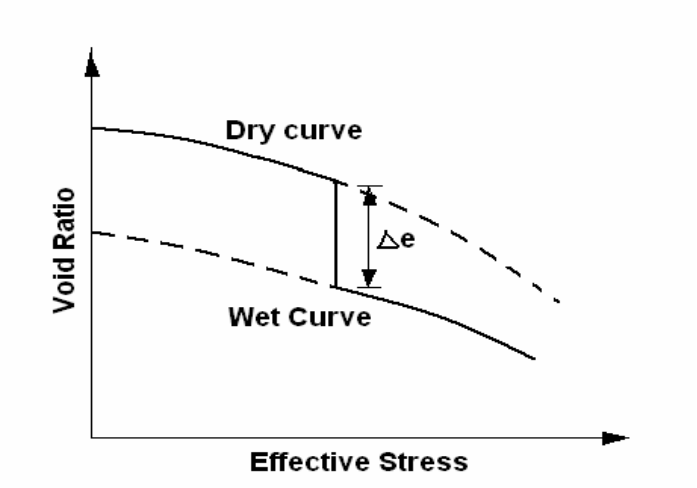

Figure 4. Modeling of the hydro-collapse due to the wetting of dry soil.

Lesturgez et al, (2004) has showed that in his observations, there was no significant difference between dry and wet curves at the starting of the experiment (at zero stress), but in our observation the dry curve has the highest void ratio where as the wet curves have the void ratios in between the undisturbed and the disturbed dry curves. He has also found that there was no significant difference between the dry curve and the wet curve at any applied stress in the case of pure sand, indicating the collapse to be insignificant and the collapse resulted from the water induced was always in between the dry and wet compaction values. In the initially dry soil, the collapse to be expected upon wetting depends on substrate properties such as soil density, pore size, particle size distributions, stress state, and stress changes (Alawaji 2001). Another soil property that affects the magnitude of settlement is clay content. Assalay *et al.* (1998) has showed that the magnitude of collapse increased with the clay content in the soil, which was up to 25 % increase. This increase in the collapse magnitude due to the clay content was also observed by Lesturgez *et al.* (2004). Loess soils undergo dynamic changes with the change in soil moisture content.

In arid and semi-arid regions, vast areas such as Saudi Arabia are covered with collapsible soils. The loess soils are sensitive to variation in water content, and display compression behaviour upon wetting (collapse), both under overburden stresses and under external loads. Wetting induces additional collapse settlement in many geotechnical applications (Dijkstra *et al.,* 1994). Excessive irrigation and broken pipes are among the most common sources of soil wetting. The dry compacted and soaked soil conditions are the most appropriate representation of wetting induced collapse potential in arid environments. Sheheta, (1997) has shown that the potential of the collapse decreased with the increase in initial soil dry density. This is because it takes a longer time for water to penetrate the voids within the dense samples. The wetting process induced an irrecoverable collapse in elastic and elasto-plastic regions of the stress.

Modeling the behaviour of soils sensitive to hydro-collapse is still in its early stages. Computer models have been used to model the soils under saturated conditions. Where as for the unsaturated loess soils, the use of computer models are difficult due to the complex collapse nature. To overcome the difficulties of complex collapse nature particle packing perspective was considered. A packing value of 0.78 was confirmed by Assallay *et al.,* (1996). With the knowledge of the particles packing we can know weather the soil is prone to collapse or not. Using this, work is currently being conducted to develop a model (CRISP90) to analyze the behaviour of collapsing loess soils (Miller *et al*, 1998).

2.3 Consolidation Curve

A graphical procedure developed by Casagrande (1936) is regarded as a standard method. He developed this method empirically from a large number of tests on different types of soils and used it to derive the pre-consolidation load with a satisfactory degree of accuracy. Figure 3 demonstrates Casagrande's procedure using data from a uniaxial compression test: One determines first the position of the virgin compression line (VCL) with a sufficient number of points. Then one determines on the preceding branch the point T that corresponds to the smallest radius of curvature, and draws through this point a tangent (Tt) to the curve, and a horizontal line (Th). The angle between these two lines is then bisected (Tb), and the point of intersection of this bisecting line with the virgin line determined, which approximately corresponds to the pre-consolidation load (P) of the soil in the ground. Casagrande (1936) determined the point corresponding to the smallest radius of curvature visually. The visual determination is very subjective and scale-dependent.

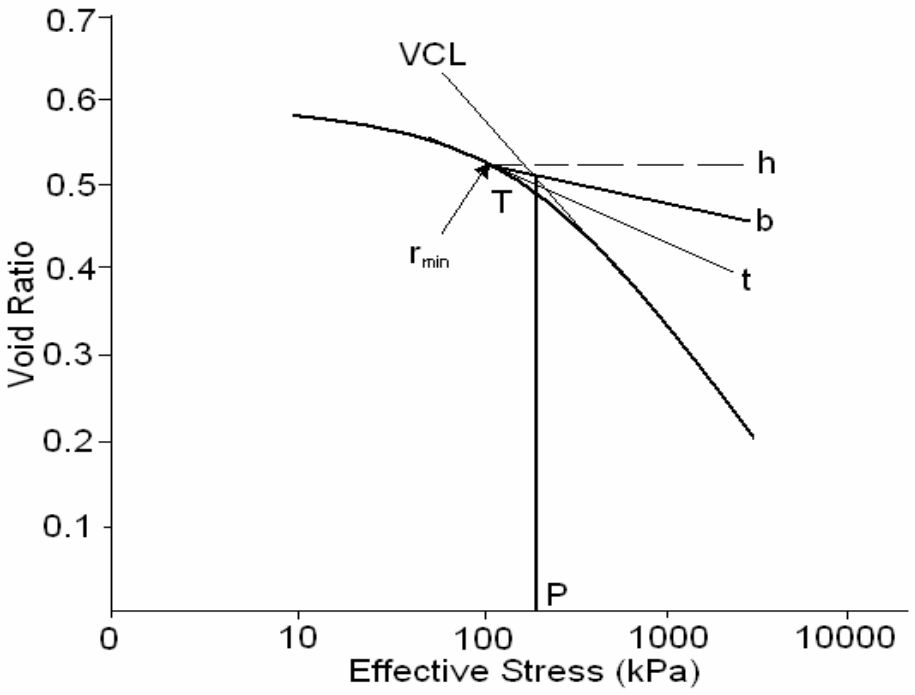

Figure 5. Graphical method (Casagrande, 1936) for determination of the pre-compression stress. The intersection of the virgin compression line and the bisecting line b corresponds to the pre-compression stress (P).

Another method was proposed by Silva (1970) to determine pre-consolidation stress (P), which is widely used in Brazil. Similar to Casagrande's (1936) method, Silva's method uses an empirical construction from the *e* – log P curve, where *e* is the void ratio and P is the vertical effective stress. The pre-consolidation stress is determined graphically from the oedometer test data as shown in Figure 6. First the horizontal line (AB) is drawn, which represents the maximum void ratio (e_o) value. The virgin compression line (CD) has been drawn which is represented by dashed line and is extended till it meets the AB line. From the point at which the point at which the virgin compression line meets the maximum void ratio line, a line is drawn in vertically downward direction till it meets the curve, which is represented by E. From point E a horizontal line is drawn which extends up to the virgin compression line (F). The effective stress value at the point F is the pre-consolidation stress (P).

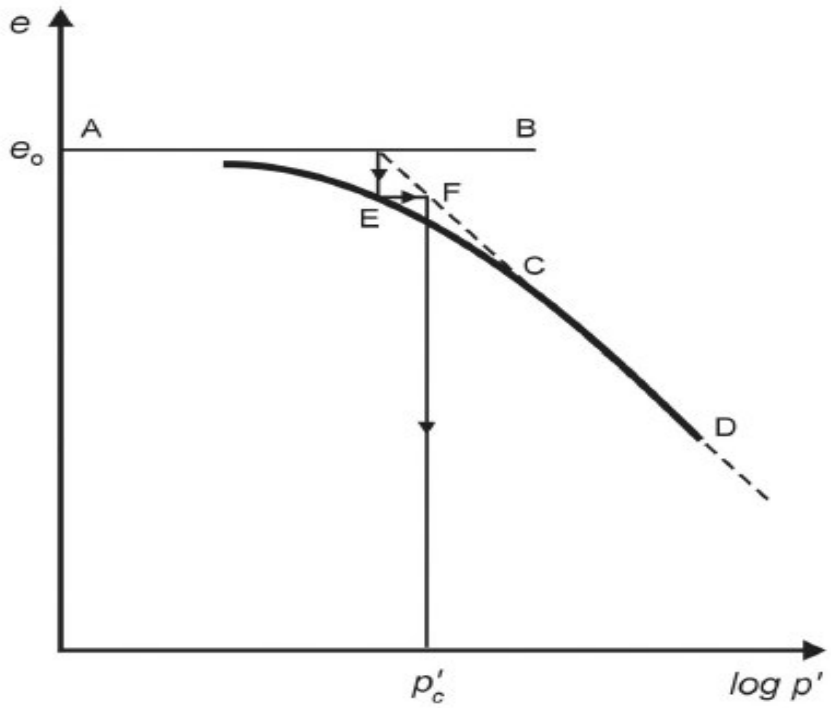

Figure 6. Determination of pre-consolidation stress value using the Silva (1970) construction.

As we know that the casagrande 1936 method is highly subjective as it varies from person to person in finding out the point of maximum curvature. This problem is solved by the Silva (1970) method. The pre-consolidation stress value obtained using Silva (1970) method is not subjected to interpretation. Therefore, the value obtained will be same always and is not prone to errors. Silva (1970) method is independent of the drawing scale, whereas the Casagrande (1936) method is scale dependent.

We used the casagrande (1936) method in determining the pre-consolidation stress values. The values determined were subjective to prone some errors due to the reason that the point of maximum curvature cannot be found exactly. So we also found out the maximum and the minimum stress values such that the pre-consolidation stress value obtained will always be in between these two values. Figure 7 shows the procedure how to determine minimum and maximum stress values graphically. A is the point where the curve has minimum radius of curvature. The minimum compression value σ_{vmin} is found out graphically at the point where the maximum void ratio (ε_{max}) line meets the virgin compression line (VCL), where as the maximum compression value σ_{vmax} is found out at the point where the virgin compression line is deviated from the compression curve and the most probable σ_v value suggested by Casagrande is at the point where the bisector AD meet the virgin compression line.

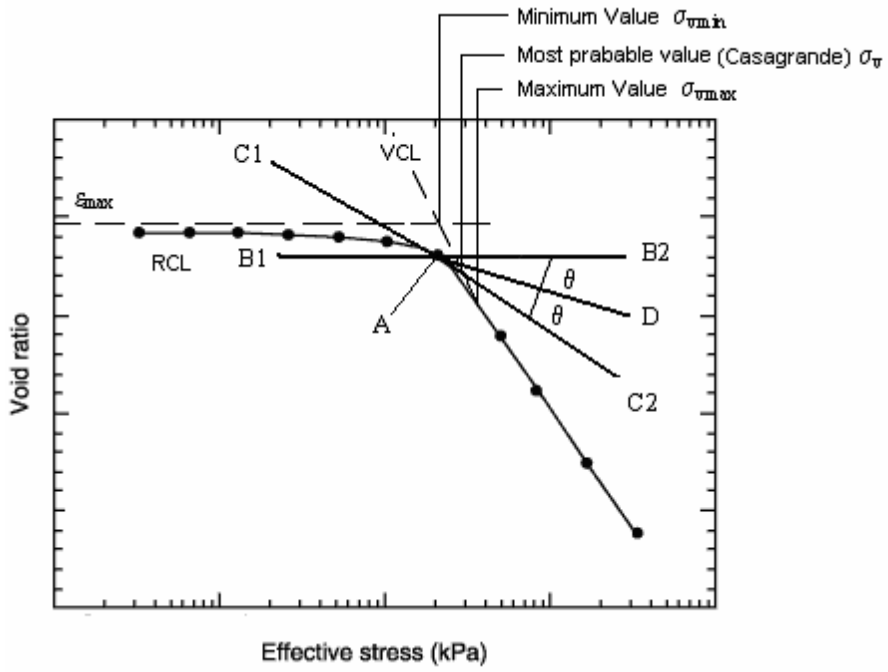

Figure 7. Determination of the most probable compression value of the soil

2.4 Curve Fitting

Curve fitting is one of the important steps in determining the pre-consolidation stress value. The basic mathematical description of soil compaction is the relationship between the stress and void ratio or bulk density etc and drawn on a semi-logarithmic graph. In which the effective stress is drawn on the logarithmic scale. In this logarithmic model it is not possible to define the void ratio or bulk density values at zero stress.

To overcome this problem Bailey *et al.,* (1986) developed a three parameter equation (Eq. 1), which was in disagreement with experimental observations. Assouline et al., (1997) modified this equation with only two parameters. Further Fritton (2001) gave a new equation with three parameters (Eq. 2), in which he has shown that the bulk density is a function of applied stress plus one but in the terms of physics, bulk density is only expressed as a function of applied stress. Assouline (2002) modified his old equation from 1997 and gave a new equation with three parameters (Eq. 3).

$$\ln(\rho) = \ln(\rho_o) - (a + b\sigma)(1-\exp^{-c\sigma}), \quad [1]$$

where ρ_o is soil bulk density at zero stress, and a,b,c are empirical parameters.

$$\rho = \rho_m - (\rho_m - \rho_o)\{1 + [\alpha(\sigma + 1)]^n\}^{-m} \quad [2]$$

where ρ_m is soil particle density and α, n, m are empirical fitting parameters.

$$\rho = \rho_o + (\rho_{max} - \rho_o)[1 - \exp^{-(k\,\sigma)\omega}]; \; \omega > 0 \quad [3]$$

where ρ_{max} and k are fitting parameters and ω as the third parameter.

Further Baumgartl, (2002) has showed that it is possible to use a mathematical formulation of the model of water retention curves to describe the volume change in soils. The water retention curves are commonly modeled using the van Genuchten, (1980) equation. He modified the van Genuchten (1980) equation by replacing moisture ratios by void ratios which is given in Equation [7]. All the equations from Equation 1 till Equation 3 and Equation 7 are derived based on the assumption that the curve has sigmoidal shape (classical S-curve).

3. Materials and Methods

3.1 Test Material

The glacial till used for the experiments was sampled in the Lusatian lignite-mining district located about 100 km southeast of Berlin, Germany. Since the last decade, this material has been used to restore arable land which has been consumed due to opencast lignite mining operations. The glacial till used for the experiments derived from the sediment layer of Warthe sub-stage of the saalian glaciation. This layer stretches exclusively over the mining area having a mean thickness of approximately 20 m. Sediment samples were taken from the pre-cut section of the open-cast pit from a depth of 3 m to 10 m. The glacial till was of sandy texture, coherent structure and slightly calcareous. The glacial till has been classified as loamy sand (USDA soil texture classification).

3.2 Approach

The approach of the recent work was to evaluate the impact of disturbance and water-induced compaction on the pre-consolidation load of the glacial till. Pre-consolidation load is defined as the largest overburden stress to which a soil has been exposed. The pre-consolidation stress divides the soil compression curves into a region of small elastic deformation (recompression), which defines the soil management history and into a region of plastic deformation (virgin compression) (Holtz and Kovacs, 1981). The value of pre-consolidation load is found out at the point where the stress-strain curve experiences a change in gradient (Figure 8). To determine the effect of increasing load with respect to the depth, pre-consolidation load was measured on undisturbed as well as disturbed soil samples from 4 m, 6 m, 8 m and 10 m depths.

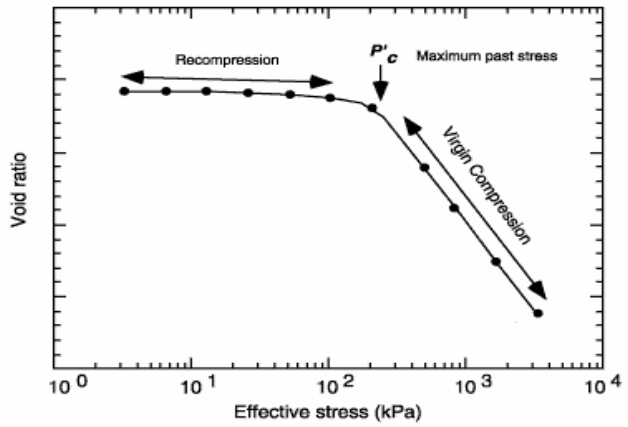

Figure 8. Elastic and plastic deformation of the consolidation curve

To get an idea of the soil characteristics before excavation, in the first step parameters like soil bulk density, calcium carbonate content ($CaCo_3$), grain size distribution and water retention characteristics were measured for the whole profile.

In the second step the impact of disturbance on the stability (pre-consolidation load) of the glacial till was evaluated. This comprised three sub-steps. The first comprised of determination of the stress-strain behaviour in undisturbed soil samples reflecting the undisturbed conditions. In the second step the stress-strain behaviour was measured on dry soil samples, which reflects the situation during summer when the glacial till dries during transport on the conveyor belt before deposition. With the specific saturation of dry pre-loaded soil samples, in the third step the effect of saturation and re-compaction by rain was simulated.

On the basis of the stress-strain behaviour experiments and against the background of the soil properties, the goal of this work was to model the effective stress in the re-wetted soil. It should be shown that the stress corresponds with the load of the overlying soil column.

The above described approach was exemplarily carried out for undisturbed sediment samples and also for disturbed dry sediment samples from 4 depths (4 m, 6 m, 8 m, and 10 m) where as due to pragmatic reasons the disturbed dry and saturated sediment samples were only tested at depths of 4 m and 8 m.

3.3 Sampling scheme

Sediment samples for the different investigations were taken from the excavation site about 1500 m west to the eastern end of the glacial high terrace ‘Hornoer Berg’ from a depth of 3 m to 10 m depth. The sediment samples were taken such that they represent the characteristics of the investigated glacial till layer. Table 1 gives an overview of the sediment samples which were taken from the glacial till layer for various laboratory investigations.

Table 1. Sampling Scheme

Depth	Carbonate	Soil bulk density	Pre-consolidation load			Water Retention	Grain size distribution
(cm)	(%)	g cm^{-3}	Undisturbed	Disturbed	Re-wetted		
300		X					
400	X	X	X	X	X	X	X
500		X					
600	X	X	X	X		X	X
700		X					
800	X	X	X	X	X	X	X
900		X				X	X
1000	X	X	X	X		X	X

3.4 Methods

The **Grain Size Distribution** of the sediment samples was determined using the sieve analysis for particles > 0.063 mm and the sedimentation analysis for particles < 0.063 mm (Schlichting *et al*., 1995). The sieves used for sieve analysis were 2 mm, 1 mm, 500 µm, 250 µm, 125 µm, and 63 µm.

Soil Bulk Density was estimated using the core cylinder method. Sediment samples were taken using steel rings of 100 cm^3 on the horizontal face of the pre-cut section. Five replicates were taken in intervals of 1 m, each from 3 m to 10 m depth. Soil bulk density (ρ_{soil}) was calculated from the oven-dried weight (105°C, 24 h) and the volume of the sample as follows.

$$\text{Soil bulk density} = \frac{\text{(oven dried weight – cylinder weight)}}{\text{Volume of sample}} \quad [4]$$

Void Ratio ε values were derived from bulk density (ρ_{soil}) and particle density ($\rho_{particle}$) using Equation 5. The measured particle density of 2.65 Mg / m^3 (Measured by Stock, 2005) is used in the calculation.

$$(\varepsilon) = (\rho_{particle} / \rho_{soil}) - 1 \quad [5]$$

The **Carbonate Content** was measured using a Scheibler-Dietrich apparatus (Figure 9). The Scheibler method involves the determination of the carbonate content of a soil based on a volumetric method. The carbonates contained in the sample are converted into CO_2 by adding hydrochloric acid to the sample. As a result of the pressure of the CO_2 released, the water in a burette that is de-aerated rises. The difference in level measured is an indication for the released quantity of CO_2, from which the carbonate content can be calculated. The carbonate content is expressed as equivalent calcium carbonate content. The equation for the calculation of amount of calcium carbonate and the conversion tables were taken from Barsch and Billwitz (1990).

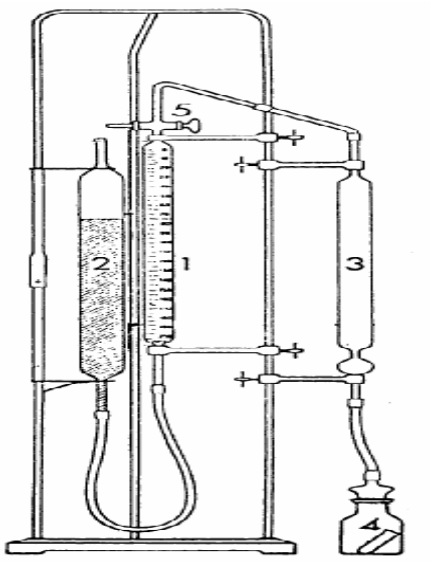

Figure 9. Schiebler-Dietrich Apparatus 1:-Graduated tube, 2:-Tube showing difference, 3:-Connecting flask and tube 1, 4:-Special Flask, 5:-Turning Knob.

The **Soil water content vs. soil water tension (pF-curve)** was measured on five replicates taken from the horizontal surface of the pre-cut section, each from 4 m, 6 m, 8 m, and 10 m depth. The relation of soil water content vs. soil water tension was measured using suction plates for the range from pF1.8 to pF2.8 and pressure chambers for soil water tensions ≥ pF3.0 (Klute, 1985). In the first method, the water is drained from the soil samples using a negative pressure difference, where the pressure will be increased in suction stages (63.1 hPa to 631 hPa) and held at each intermediate value until the water flow from the apparatus comes to a standstill state. The second method uses positive pressure difference as the air pressure is applied from top of the soil samples and the water is pushed out from soil sample to the suction plate inside the pressure chamber.

Equation [6] is given by van Genuchten (1980) for fitting the soil-water retention curves, where θ_r is the residual water content and θ_s is the saturated water content.

$$\theta = \theta_r + (\theta_s - \theta_r) / [1+ (\alpha h)^n]^m; \; m = 1 - 1/n. \qquad [6]$$

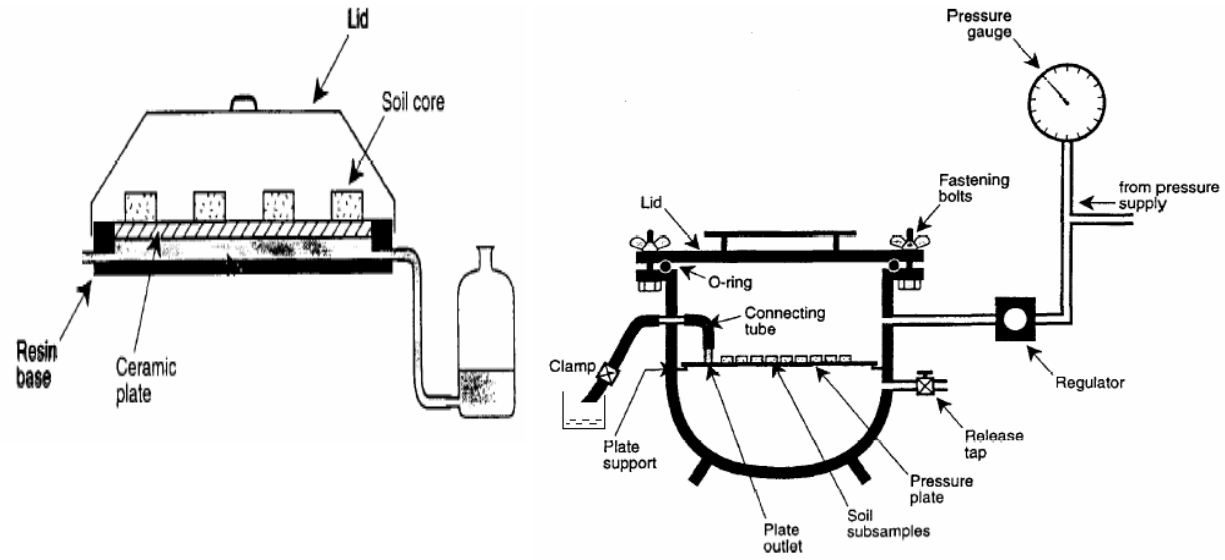

Figure 10. Ceramic Plate and Pressure Chamber

The **Stress-Strain Behaviour** of the samples was measured with a uniaxial compression apparatus, also referred as Oedometer. Stress history is usually determined by interpreting the results from Oedometer tests to obtain the pre-consolidation stress proposed by Casagrande (1936). This method is based on the assumption that the soil experiences a change from elastic deformation (reversible, small gradient) to plastic deformation (irreversible, high curve gradient). In order to obtain the stress-strain relationship, the load is usually increased stepwise (sequential loading). The load is typically applied for 24 hours (or longer) per load step. Due to the pragmatic reasons in our investigations a time step of 12 hours was used as the settlement was about 99% in this time period. The applied loads were 10, 20, 30, 50, 100, 200, 300, 500, 1000, 2000 and 2500 kPa. Two replicates were used to determine the stress-strain behaviour of all sediment as well as disturbed one. For the disturbed dry and re-wetted sediment samples were loaded with 0, 5, 10 and 20 kPa load respectively before the sediment samples were wetted. Before pre-consolidation load is determined the compression curves were fitted to the void ratio data by iterative nonlinear regression procedure on the basis of the model suggested by van Genuchten (1980).

In our work we have modified the van Genuchten (1980) equation to fit the curves for pre-consolidation load. We modified the equation by interchanging the symbols θ_r with the minimum void ratio value (e_{min}) and θ_s with the maximum void ratio value (e_{max}). The equation is the transformed as given in the equation [7].

$$e = e_{min} + (e_{max} - e_{min}) / [1+ (\alpha\sigma)^n]^m; m = 1 – 1/n. \quad [7]$$

In Equation [7], ε_{max} is the void ratio at zero stress, ε_{min} is the minimum void ratio and σ is the applied stress. α and n are empirical fitting parameters. In all cases ε_{min} was fitted, while ε_{max} was both set to the effective void ratio, which represents the status of the sample after water-induced collapse and relief of the strain, and best fitted, respectively.

The pre-consolidation load was calculated graphically using Casagrande's (1936) method (see Chapter 2). The undisturbed soil samples were saturated and drained to a water tension of 63.1 hPa on suction plates. The samples were then placed in oedometer and different stresses were applied. The resultant height difference of the sample at each stress level was recorded. In the case of disturbed dry samples the samples the samples were subjected to different stresses in the oedometer and for the disturbed saturated samples, the samples were placed on the suction plates with different applied pre-loads (0 kPa, 5 kPa, 10 kPa, 20 kPa) at a water tension of 63.1 hPa. Then the samples were placed in oedometer and were subjected to different stresses.

4. Results

4.1 Substrate properties

The **Texture** of the glacial till used for the experiments was classified as loamy soil on the basis of USDA soil texture classification. The detailed grain size distribution is plotted in the form of the graph as shown in Figure 11 (see also Appendix 1). The sieve analysis results showed that the glacial till was uniformly distributed with in the soil profile irrespective of depth; however there was a slight increase in silt and clay content with depth. The results devastated that there was no effect of grain-size distribution on the pre-consolidation stress values.

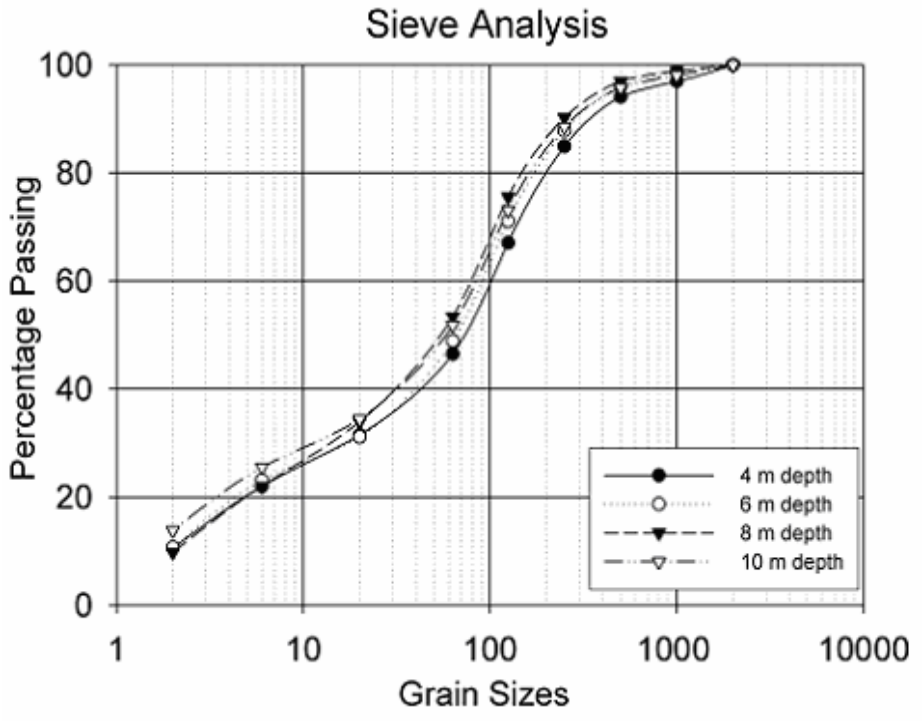

Figure 11. Grain size distribution of the investigated glacial till layer with depth at the pre-cut section of lignite mining pit Jänschwalde

Results of **Soil Bulk Density** were displayed in Figure 12. Between 3 m and 10 m the mean soil bulk density values were in the range of 1.9 to 2.0 g cm^{-3} respectively. The bulk density does not increase steadily with depth. We found that the soil bulk density increased from 3 m to 4 m and then decreased till 7 m depth, where the lowest soil bulk density value was recorded. Then bulk density again increased from 7 m till 10 m depth, however the increase from 9 m to 10 m was only small. The standard deviation values in general were small.

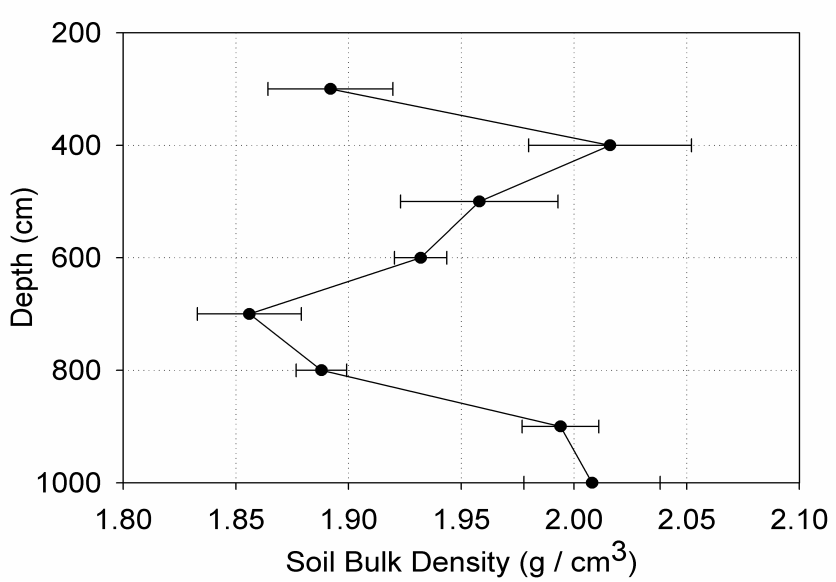

Figure 12. Mean soil bulk density of the investigated glacial till layer with depth at the pre-cut section of lignite mining pit Jänschwalde (5 replicates from each depth)

Results of **Soil Water Content** were plotted in form of a graph as shown in Figure 13 (see also Appendix 2). The effective mean water content values measured from 3 m to 10 m were in the range of 0.15 to 0.29 cm^3 cm^{-3}. We found an increase from 3 m depth till 4 m depth and decrease till 8 m depth; however the increase in general was very small and were in between the values obtained from 3 and 4 m. From 8 m till 10 m depth water content rises again, where the maximum value was recorded at 10 m depth which is the maximum soil water content value and further with the increase in depth till 12 m we have observed the water flowing out of the profile (pre-cut section). The standard deviation values were small.

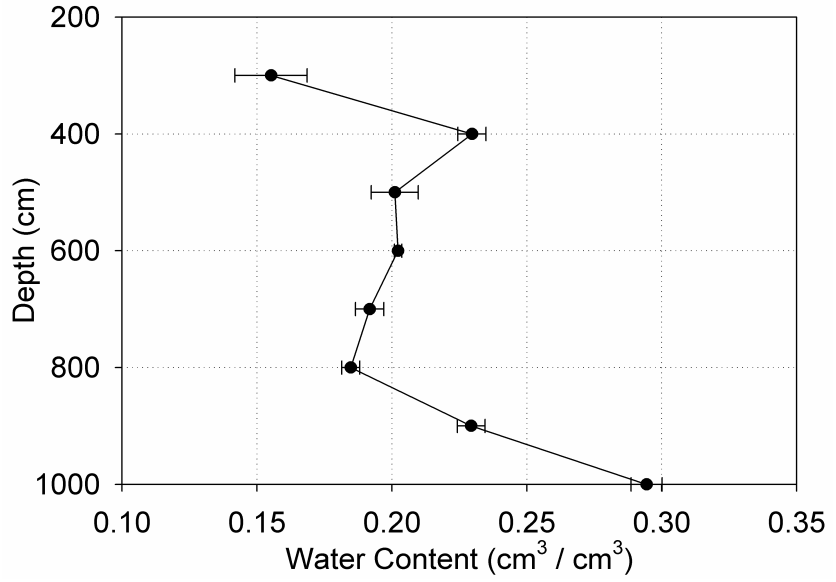

Figure 13. Soil Water Content of the investigated glacial till layer with depth at the pre-cut section of lignite mining pit Jänschwalde (5 replicates from each depth)

The **Carbonate Content** divided the profile clearly into 2 different layers. First layer was free of carbonate having a mean value between 0.07 % and 0.1 %. The second deeper layer was characterized by the mean values of about 5.3 % to 5.4 %. The alteration was between 6 m and 8 m depths. The carbonate content distribution with respect to the depth is shown in Appendix 3.

In Figure 14, the graphs were plotted as **Water Content vs. the Soil Water Tension**. The profile could be dissected into two main types: 1) curves obtained from 4 m and 10 m depths, 2) curves obtained from 6 m and 8 m depths. We observed that the samples from 4 m and 10 m do not have coarse pores as the drainage of the samples start from the point above field capacity, where as the samples from 6 m and the 8 m have coarser pores as the drainage starts below the field capacity value (see also appendix 4).

At 4 m depth the curve shows a steeper gradient and the difference in the water content values when the sample is saturated and at the point of permanent wilting point was 0.15 cm^3 cm^{-3} only. At 6 m depth though the drainage starts from the saturation point, the curve shows a steeper gradient. At 8 m depth the samples displayed maximum saturation water content and the increase in drainage was gradual. At 10 m depth there is not much of drainage till the 200 hPa and then the drainage starts increasing gradually. On the basis of water retention curves, the saturated water content, field capacity and permanent wilting point were calculated and are given in table 2. Saturated water content is defined as the water content which completely fills the voids between the soil particles (1 hPa or pF0). Field capacity is defined as the difference between the plant available water and the saturated water content (63.1 hPa or pF1.8). Permanent wilting point is obtained when the plants cannot uptake water from the soil, thus the water available for plant growth exists between the range of field capacity and permanent wilting point (15849 hPa or pF4.2).

Table 2. Values of saturated water content, field capacity, permanent wilting point at different depths

Depths	Saturated Water Content	Field Capacity	Permanent Wilting Point
4 m	0.2304	0.2275	0.0847
6 m	0.2542	0.2120	0.0618
8 m	0.3021	0.2242	0.0524
10 m	0.2654	0.2609	0.0588

Swelling of the samples was observed when the samples were completely saturated on the suction plate, especially from the 8 m depth samples. Shrinkage was also seen in the samples from 4 m depth when the samples were completely drained at pF4.2.

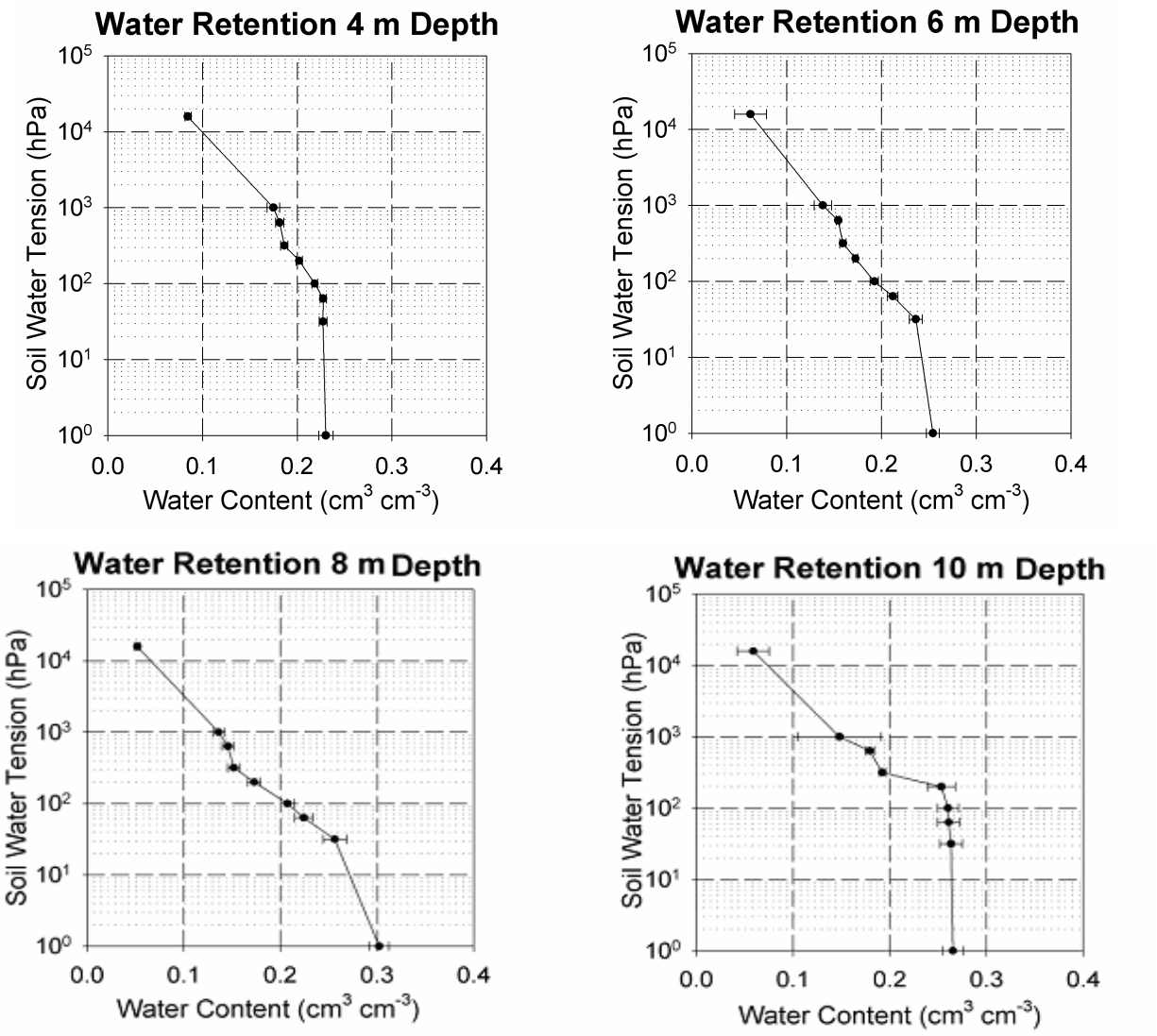

Figure 14. Water retention curves (pF-Curve) at different depths of the pre-cut section in lignite mining pit Jänschwalde (5 replicates from each depth)

4.2 Stress-Strain behaviour

Stress-strain behaviour was determined using the Oedometer apparatus. The data obtained was plotted in the graph using the data logarithmic value of stress (log σ) vs. the void ratio (ε). To know the trend of stress-strain behaviour with respect to the mining operations, 3 different approaches 1. Undisturbed, 2. Disturbed (air dried), and 3. Disturbed (air dried) and saturated were used. In case of the disturbed and saturated samples step 1, step 2, step 3, step 4 are used instead of the stresses 0 kPa, 5 kPa, 10 kPa, 20 kPa that were applied during the water-induced compaction process.

4.2.1 Stress-strain behaviour under undisturbed conditions

Figure 15 shows the stress-strain behaviour of the undisturbed samples. The four different graphs were drawn for different depths with two samples each respectively. The samples from 4 m depth show similar curves but the difference between the initial void ratios is more then the difference in the final void ratio measured. The samples from 6 m depth and 8 m depth have the same curve shapes and there was no difference in the void ratio values. For the samples from 10 m depth, the curves show similar shape and the difference between the void ratio values was constant through out from the starting point till the ending point (see also Appendix 5).

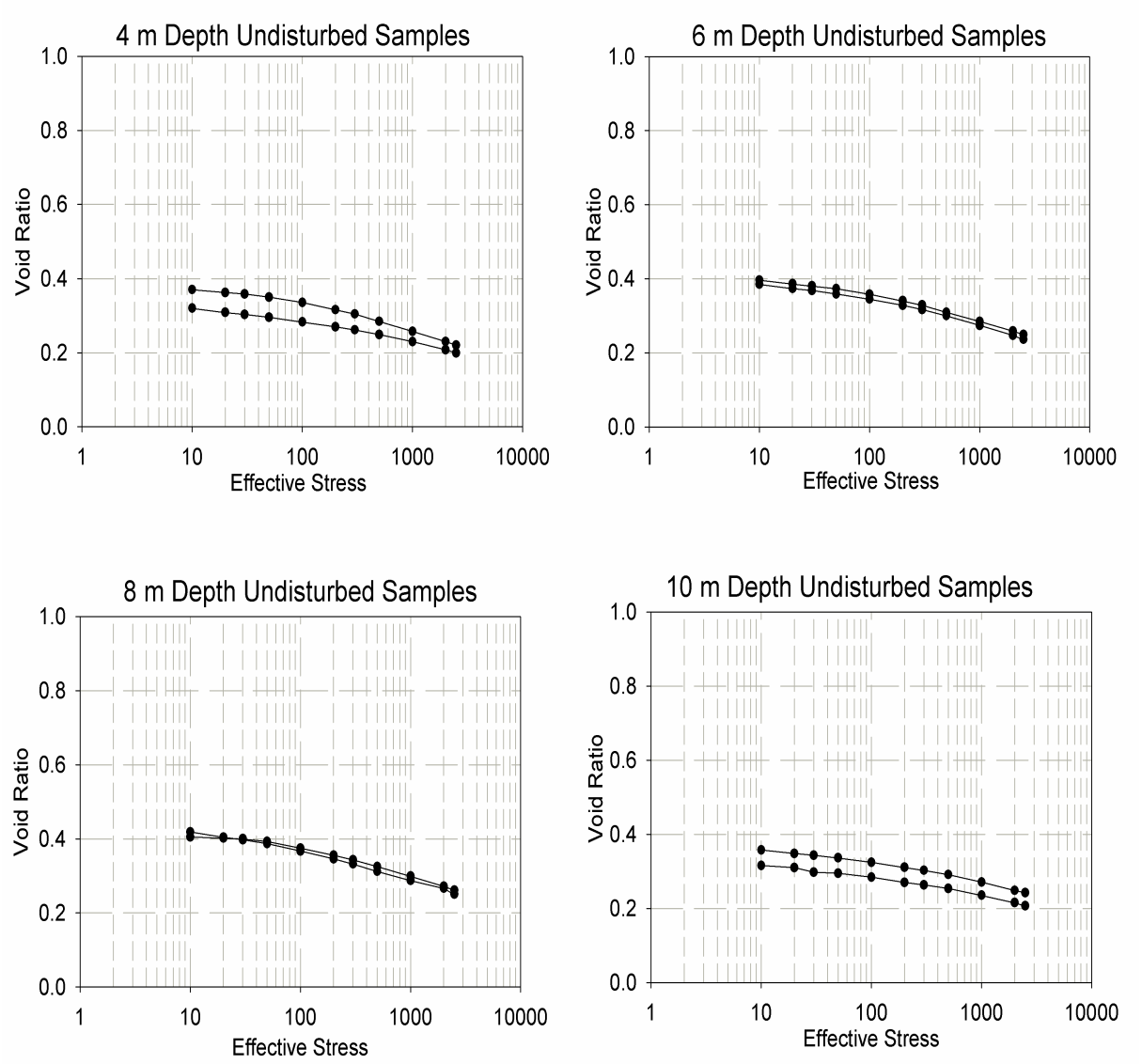

Figure 15. Stress-strain relationship at different depths of the pre-cut section in lignite mining pit Jänschwalde (2 replicates from each depth)

4.2.2 Stress-strain behaviour of samples under disturbed dry conditions

Figure 16 shows the stress-strain behaviour of the dry disturbed soil samples which were sieved in air dried conditions. Which simulates the situation when the soil has been excavated, transported on the conveyor belt where the soil water evaporates, becomes dry and is then deposited. Four different graphs were drawn for different depths with two samples respectively. In general the samples have a varying void ratio values ranging from 0.7 to 1.0 in the starting and have an almost same value ranging in between 0.4 and 0.5 at the end. In the graph at 4 m depth it can be observed that the void ratio of the two samples are not same at the beginning, however the void ratio value is same at the final stress applied. The graphs from 6 m depth and 10 m depth look similar but the void ratio values of 6 m depth were higher then that of 10 m depth samples. The graphs at 8 m depth look similar with not much change in the difference of void ratio values in the beginning and also in the end (see also Appendix 6).

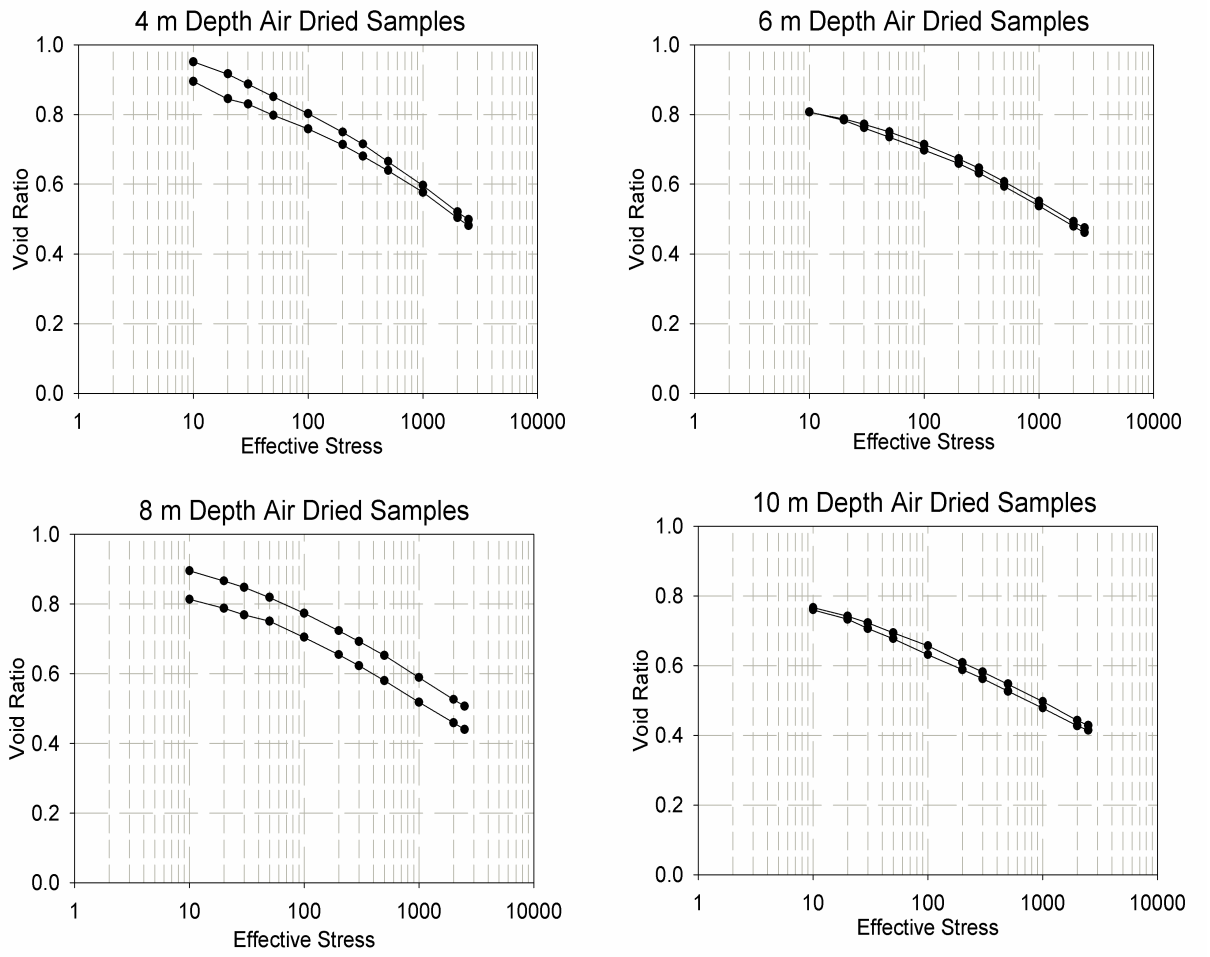

Figure 16. Stress-strain relationship of the crushed sample at different depths of the pre-cut section in lignite mining pit Jänschwalde (2 replicates from each depth)

4.2.3 Stress-strain behaviour of disturbed and subsequently saturated samples from 4 m depth

Figure 17 shows the stress-strain behaviour of the disturbed and saturated samples from 4 m depth with different applied stresses, which simulates the situation when the soil is rewetted by precipitation in the winter season after dry deposition. In general we observed that there was a decrease in the initial void ratio value with the increase in the preloaded stress, however the final void ratio values were almost equal. The graphs of step 1 (0 kPa) stress look completely different but the void ratios values at the starting point and the ending point are same. The graphs of step 2 (5 kPa) and step 3 (10 kPa) stress look similar like an classical S-curve. There was no difference in void ratio values in case of step 2 samples, whereas in case of step 3 samples the difference in void ratio values was different at all the point measured. The samples of step 4 (20 kPa) stress showed same values in the beginning but have a difference in void ratio value at the end (see also Appendix 7).

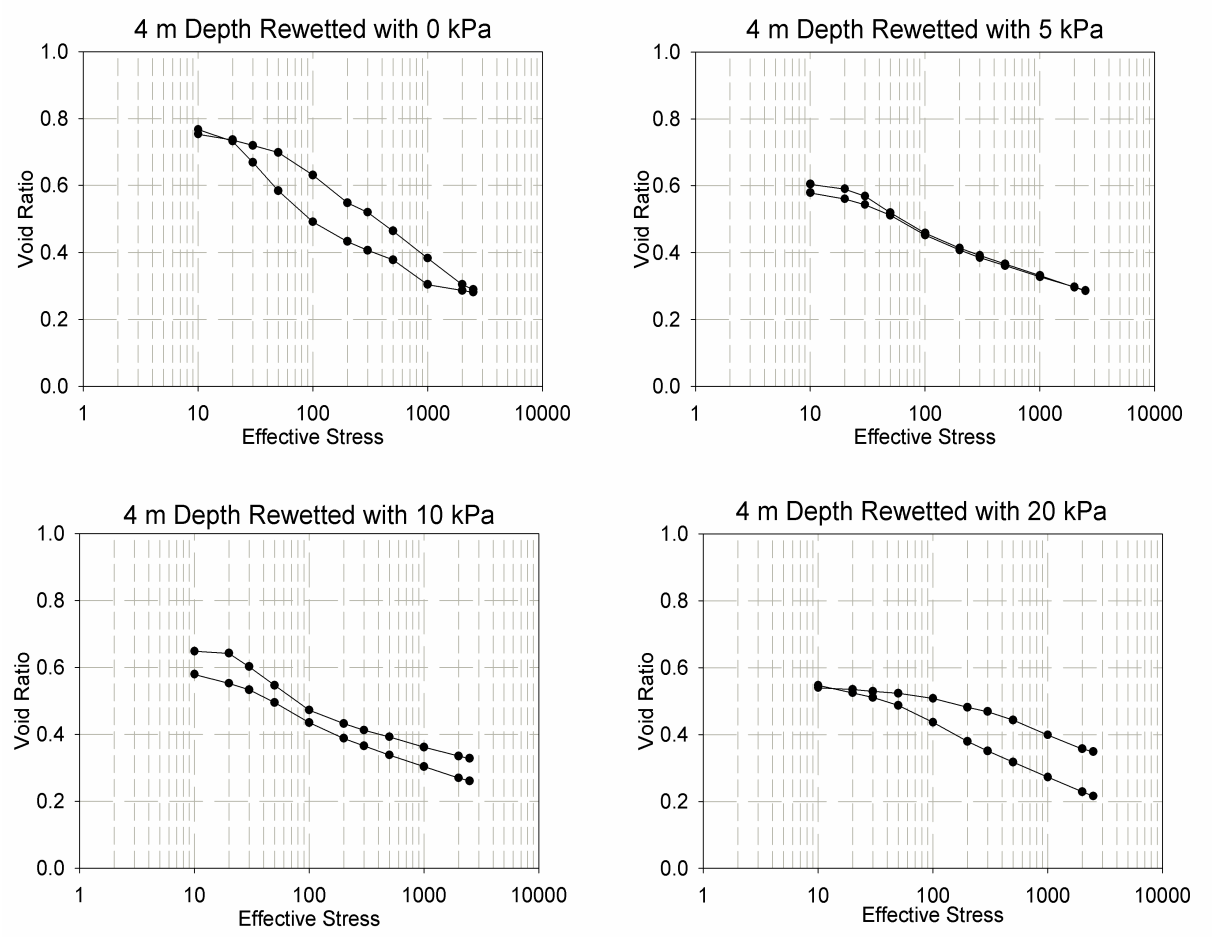

Figure 17. Stress-strain relationship of the disturbed wetted samplse at 4 m depth with different stresses taken from the pre-cut section at lignite mining pit Jänschwalde (2 replicates at each stress)

4.2.4 Stress-strain behaviour of disturbed and subsequently saturated samples from 8 m depth

Figure 18 shows the stress-strain behaviour of the disturbed and saturated samples from 8 m depths with different applied stresses. In general we observe that there is a decrease in the initial void ratio value with the increase in the preloaded stress, however the final void ratio values were almost equal. The graphs of 8 m samples of step 1, step 2, step 3 stresses do not show any difference in the initial and the final void ratio values, where as the graph from the 8 m depth with the step 4 stress, we observed a slight difference in the initial and the final void ratio values (see also Appendix 8).

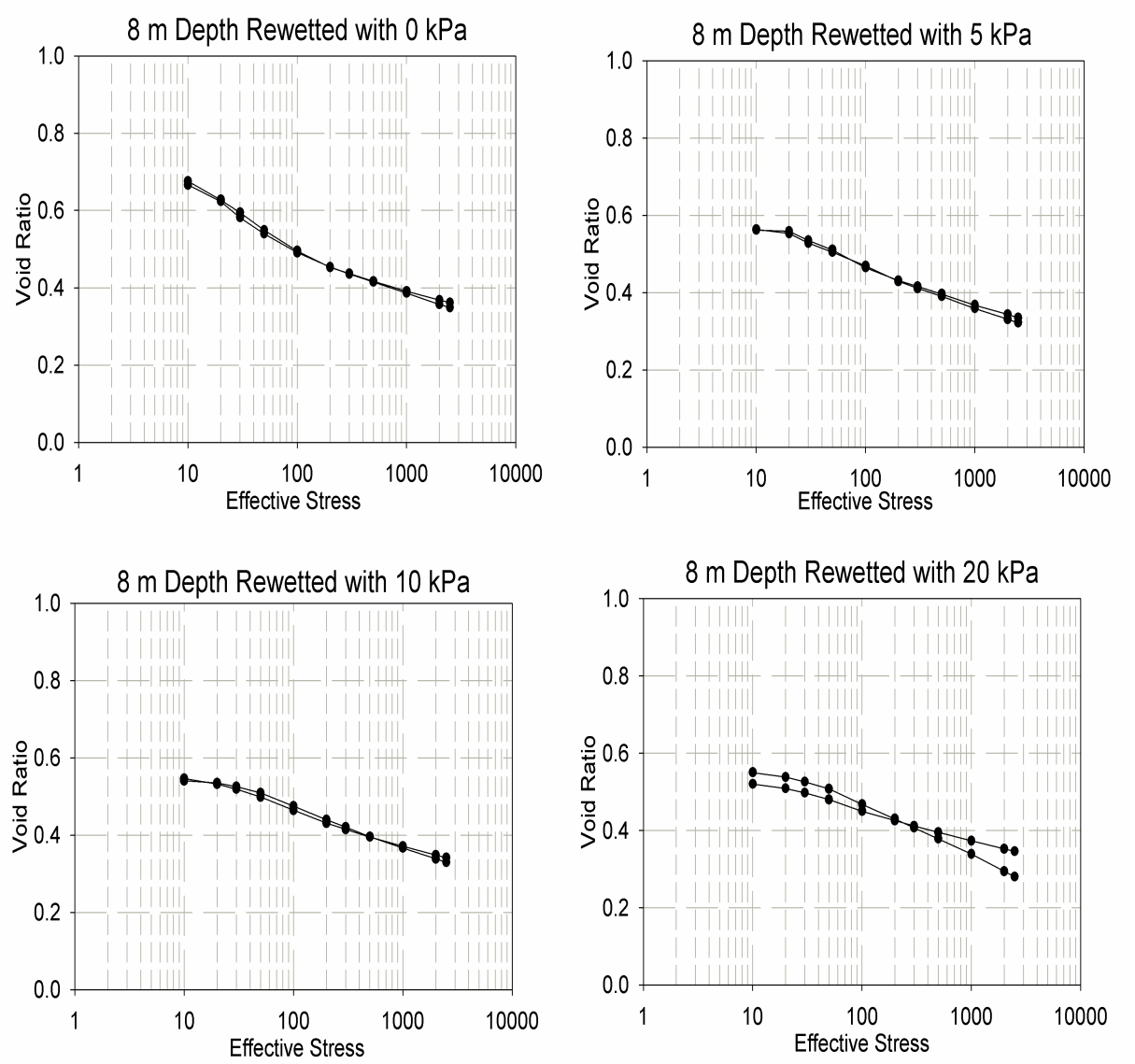

Figure 18. Stress-strain relationship of the disturbed wetted samples at 8 m depth with different stresses taken from the pre-cut section at lignite mining pit Jänschwalde (2 replicates at each stress)

4.3 Pre-consolidation Load

Pre-consolidation load was calculated using the Casagrande (1936) graphical method. The curves were fitted using the Equation [7]. The value of the e_{max}, e_{min}, σ, n and R^2 are given in the Table 28 and Table 29 (Appendix 9) for the undisturbed samples where as for the disturbed dry samples the values are given in Table 32 and Table 33 (Appendix 10). The values for the disturbed dry and saturated samples were given in Table 36 and Table 37 (Appendix 11) for the 4 m depth samples, where as for the 8 m depth samples they are given in Table 40 and Table 41 (Appendix 12). Two replicates were used in each case. Two graphs with pre-consolidation load results were plotted in each case; in first case we considered the void ratio value at 1 kPa, where as in the second case the void ratio value at 1 kPa was not considered. This was done in order to check the trend between the consolidation curves, whether there is any change or shift in the point of maximum curvature and the values of the pre-consolidation loads. The graphs were plotted with the minimum and maximum values (representing bars) and the most probable values (representing circular dots). The graphs in case of undisturbed and air dried samples were plotted as respective depths vs. the pre-consolidation load, and in the case of rewetted samples the graphs were plotted as stress applied on the samples vs. the pre-consolidation load.

4.3.1 Undisturbed Samples

Figure 19 shows the trend of the undisturbed samples at different depths. The trend looks similar whether we consider the point of minimum stress (1 kPa) or not. In the first sample the trend showed a decrease with the depth and was almost uniform like a straight line. In the case of sample 2 there was an increase in the value and then decrease. At 6 m depth there was an increase of 5 kPa observed in sample 1 and at 8 m depth also there was an increase of 15 to 20 kPa observed in both the samples when the void ratio value at 1 kPa was not considered. At 10 m depth there was only 5 kPa increase in both the samples (see also Appendix 9).

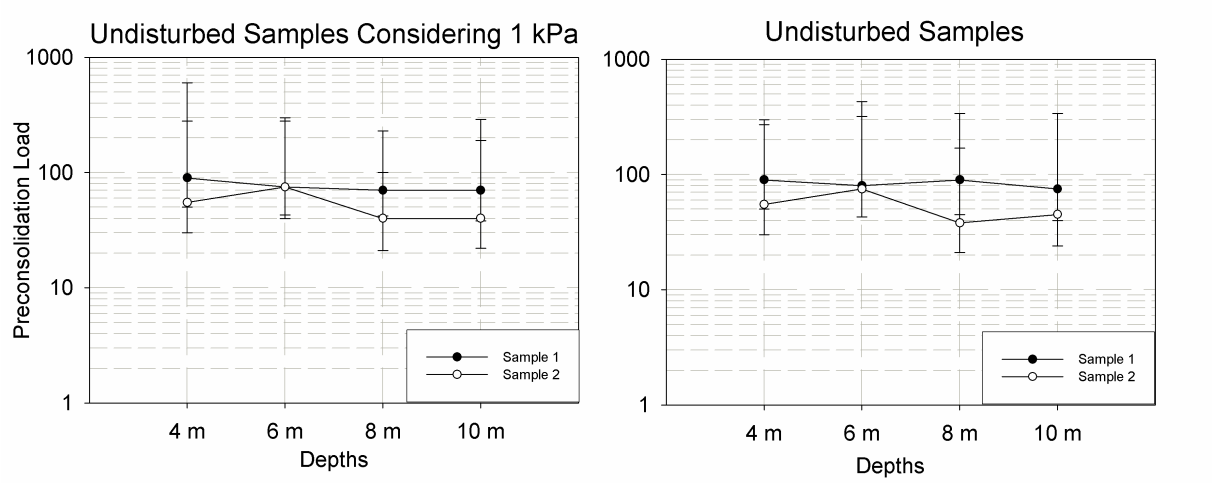

Figure 19. Pre-consolidation load calculated for the undisturbed samples (dots) and plotted in graph with minimum and maximum values (bars).

4.3.2 Disturbed Dry Samples

Figure 20 shows the trend of the disturbed dry samples representing different depths, the samples were taken from. The trend in both the graphs observed was similar. There was an increase in the value of pre-consolidation load in the beginning and then decreases in both the samples. On the contrary when the void ratio value at 1 kPa was not considered, there was only decrease observed in the second sample. At 6 m depth we observed a shift, which is about 10 kPa in sample 1, where as in sample 2 the shift is about 5 kPa. At 8 m depth there was an increase of the pre-consolidation load value by 5 kPa when the void ratio value at 1 kPa was not considered. At 10 m depth there was an increase of 3 kPa in sample 1 however there was a decrease in 3 kPa for sample 2 (see also Appendix 10).

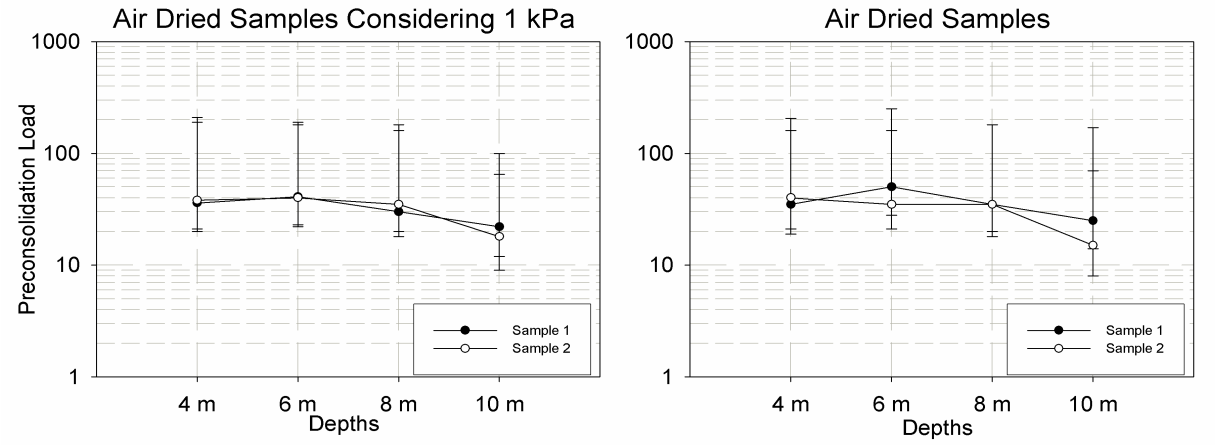

Figure 20. Pre-consolidation load calculated for the dry disturbed samples (dots) and plotted in graph with minimum and maximum values (bars).

4.3.3 4 m depth disturbed dry and saturated Samples

Figure 21 shows the trend of the disturbed wetted samples at 4 m depth. The trend is similar in both the graphs. It can be also observed that the values over-estimated the applied stress during saturation. There was a decrease and an increase observed in case of the second sample, while there was only increase observed in the sample 1 with the increase in the pre-load values. There was no clear trend observed. In general the trend showed a decrease in the value from 0 kPa to 5 kPa and constant till 10 kPa, then followed by an increase till 20 kPa. The pre-consolidation values calculated considering the void ratio at 1 kPa and also without consideration, we found that there is a certain shift in the values towards zero (see also Appendix 11).

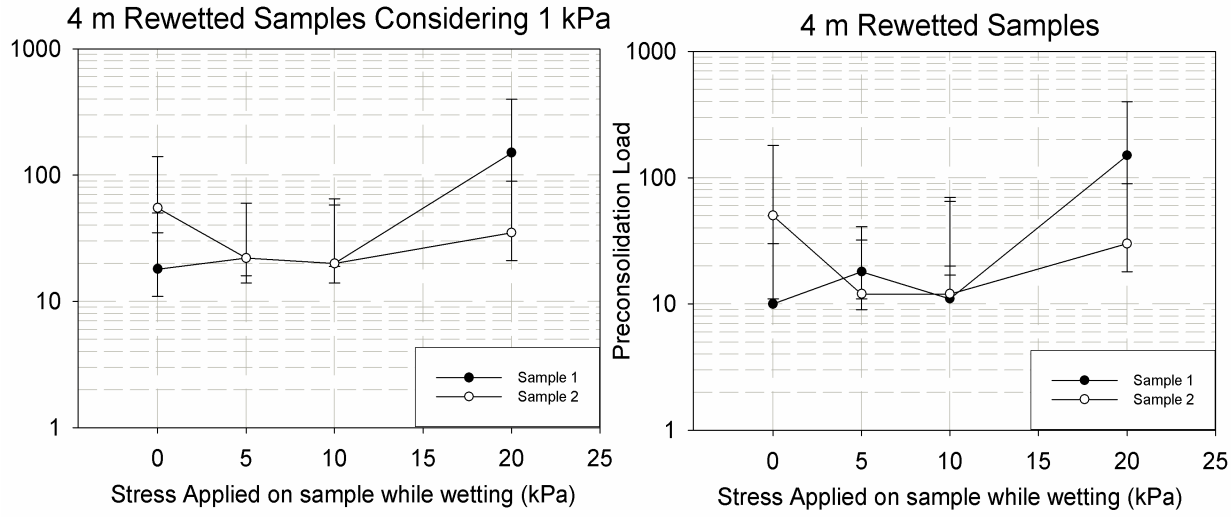

Figure 21. Pre-consolidation load calculated for the disturbed rewetted samples at 4 m depth (dots) and plotted in graph with minimum and maximum values (bars).

4.3.4 8 m depth disturbed dry and saturated Samples

Figure 22 shows the trend of the disturbed wetted samples from 8 m depth. The trend is similar in both the cases: as the stress increase the value of the pre-consolidation load also increased. We observed that the values were not over-estimated and look realistic. We also observed that the pre-consolidation values calculated considering the void ratio value at 1 kPa and also without showed a major shift in values from step1 and step 2, where as the shift was less in case of step 3 and step 4 stresses. The values looked more realistic when pre-consolidation load was calculated without considering the void ratio value at 1 kPa (see also Appendix 12).

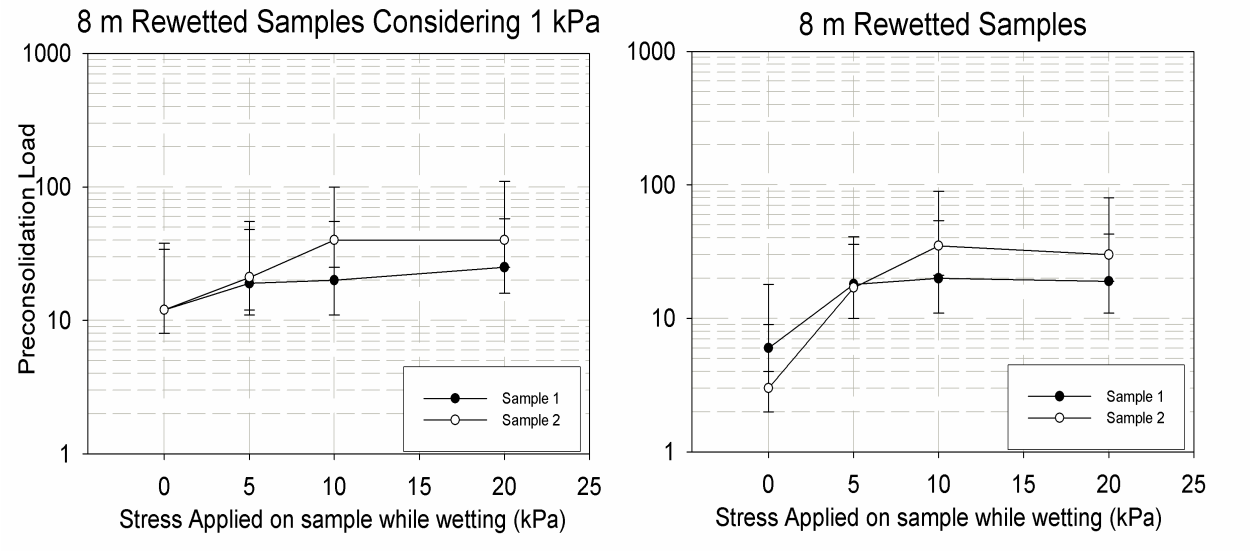

Figure 22. Pre-consolidation load calculated for the disturbed rewetted samples at 8 m depth (dots) and plotted in graph with minimum and maximum values (bars).

5. Discussion

5.1 Pre-consolidation stress vs. depths under natural conditions

The pre-consolidation stress is defined as the maximum load to which the soil was subjected in its history. In general, the overburden pressure increases with respect to depth. Figure 23 shows the values of the pre-consolidation load of the samples considering the void ratio value at 1 kPa and also without. The dashed line and the dashed line with two dots represent the estimated dry stress and wet stress. These estimated values are calculated based on the values of the mean soil bulk density (1.9 g cm^{-3}) and the water content at field capacity (0.3 cm^3cm^{-3}) of the glacial till sediment under natural conditions.

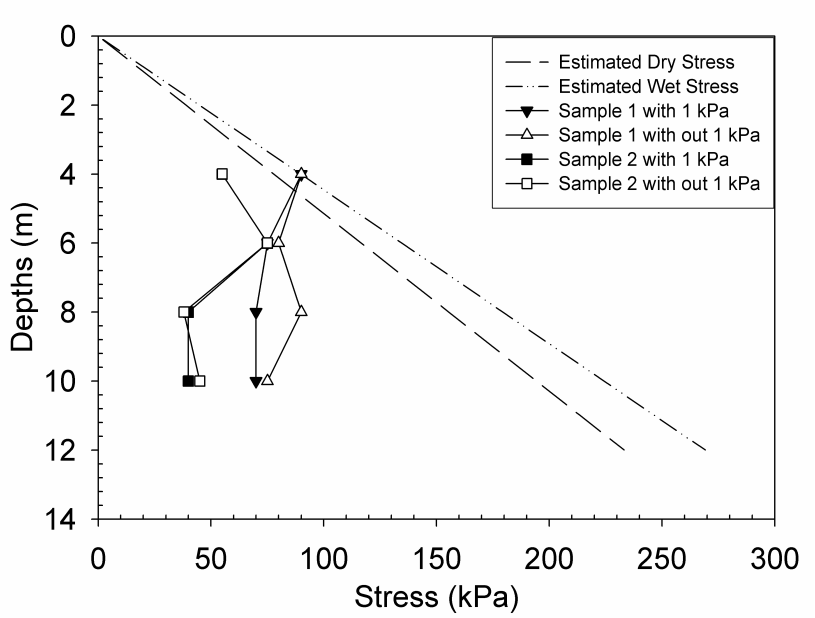

Figure 23. Pre-consolidation load under undisturbed conditions. 2 replicates considering the void ratio value at 1 kPa and without.

We expected the pre-consolidation values to be increasing with respect to the depth as shown by the estimated dry and wet stress lines, however it can be clearly seen that the results were below the expected values. At 4 m depth the pre-consolidation values lie on the vertical effective stress line except one sample, which shows smaller values. Below the vertical effective stress line, we can observe a difference in pre-consolidation load values obtained to that of the expected. The pre-consolidation values were relatively stable and the difference between the vertical effective stress line and the pre-consolidation values obtained was increasing with the depth.

This behaviour did not seem to be logical since it is assumed from the engineering science that normally consolidated soil is the soil which has been consolidated by a load equivalent to that of the existing overburden, which is represented by the straight line gradually increasing with the depth (Figure 24). Over-consolidated soil is the soil which has been consolidated by a load greater than that of the existing overburden. In this case the pre-consolidation load values of over-consolidated soils lie above the normally consolidated and meet the normal consolidation line at a certain depth, which is represented by the dashed line in Figure 24. The values in the normal consolidation will be similar to that of the vertical effective stress calculated using the bulk density and the water content values of the respective soil. Another observed gradient of over-consolidated soils is shown in Figure 24. Here a slight deflection i.e. shifting of the curve towards left and going below the vertical effective stress line in the stress values with increase in the depth can be seen, where as the stress values will be below the vertical effective stress line approaching towards zero stress with increase in depth. This shifting of the curve towards left side is caused by the concentrated external loading (footings, pillars, etc.). This explains that there was some external concentrated load acting above the pre-cut section of the glacial till.

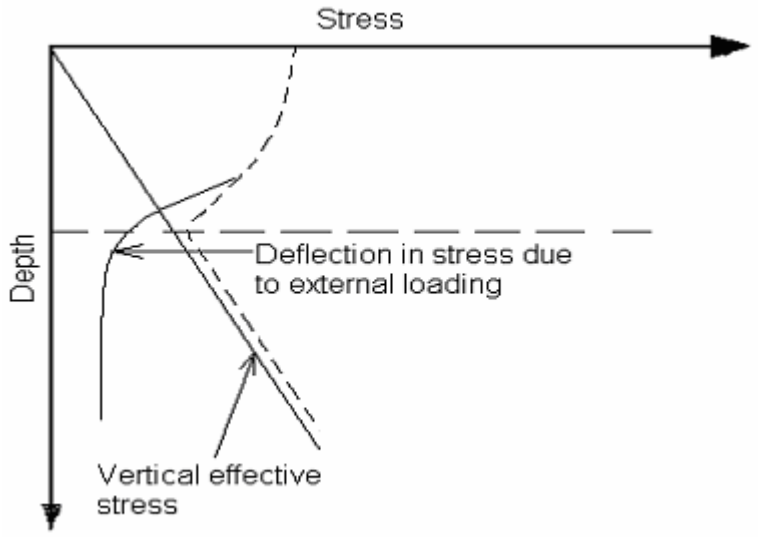

Figure 24. General normal consolidated and over consolidated under stress curves of the soil on basis of engineering science and shifting of the curves to the left due to concentrated loading.

Although no measurements were taken in the upper 4 m depths of the pre-cut section we expected to have the similar trend of curves with the samples. From 4 m depth all values were below the vertical effective stress line and approaching towards zero stress. This means that the curve has deflected from the vertical effective stress line.

In Figure 25 we show a possible prediction of the expected over-consolidation curves above the vertical effective stress lines. This is only an approximation based on the explanation from Figure 24. We assume that there will be some over-consolidation in the top till 4 m depths as the soil was used for agriculture before and also there was movement of heavy vehicles, as our samples were taken from 4 m depth till 10 m depths, and the samples from 4 m depths pass through the effective wet vertical stress line.

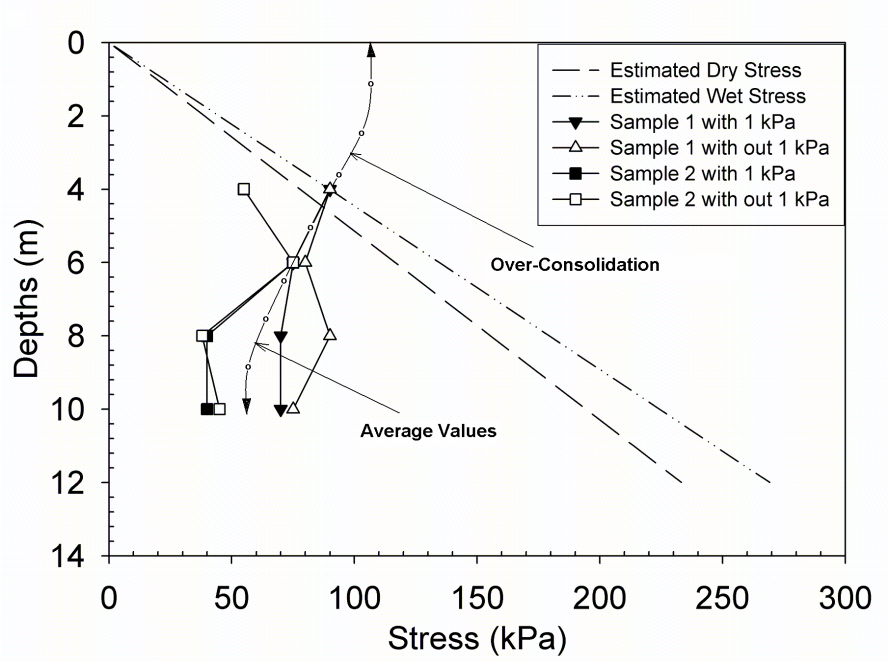

Figure 25. Showing the possible gradient of pre-consolidation on the basis of our values obtained and also the knowledge of engineering science.

Similar observations have been reported by Vrolijk *et al.* (1998) in the clay rich samples from the barbados. He has observed that the values of pre-consolidation load were less than those of the calculated normally pressured samples because there was rise in pore pressures more then that of the hydrostatic pressure before the deformation has started, and disrupted the grain contacts. This led to change in the packing stage. Bruckmann *et al.* (1997) reported a comparable observation on the consolidation data from a seabed. He observed that there was a decrease in the value of the pre-consolidation load with decreasing void ratios, showing decreasing pre-consolidation load values (excess pore pressure) with depths below the seabed. The values of over-consolidation ratio (OCR) were small less then one (the normally consolidated). The over-consolidation ratio is the ratio of the pre-consolidation stress (*P*c) to that of the overburden stress (*Po).*

$$OCR = Pc / Po \qquad [8]$$

Blum *et al.* (1995) also showed that the values of OCR were decreasing with depth, suggesting a high degree of under-consolidation in silty mud samples from the Pleistocene upper continental slope in New Jersey. The samples showed over-consolidation in the uppermost few meters and under-consolidation at high depths. He also estimated excess pore pressures of 100 kPa and 600 kPa, and vigorous gas escape during the recovery of cores in under-consolidated section. Silva (1996) found out that the deeper sediments (impermeable layer) up to 20 m depth showed normally consolidated and under-consolidated conditions, which can be correlated with finely layered sediments representing the period of high rate sedimentation. Rapid rate sedimentation within the zone of apparent over-consolidation (on top), which breaks the consolidation process, was considered as a reason for the under-consolidated conditions. The implication is that the sediments were under-consolidated due to the rapid sedimentation (Laberg *et al.,* 2000). The excess pore pressures might be having the effect of reducing effective stress in under-consolidation situations.

Another explanation of this is when group of particles with different particle-sizes are arranged in the process of sedimentation they can result in the ideal packing density in the soils. The ideal packing density is the density in which the particles are so arranged that all the particles stick together (not moveable). It is possible that this ideal packing stage in the particles is only reached by the natural conditions and with out any external loads.

The results from the Water Content vs. the Soil Water Tension showed that till the pF1.8 value from the 10 m depth the difference in drainage was not observed i.e. the samples were completely saturated, which can be due to the reason that there were no coarse pores. The value at pF1.8 represents the field capacity, which indicates the water holding capacity of the soil under natural conditions indicating a positive pore pressure.

5.2 Effects of water-induced compaction on void ratio

Void ratio is a good measure of the stresses which influences the soil volume. The mean void ratio values of the undisturbed samples, air dried samples and the disturbed dry and saturated samples are given in Table 3 and Table 4. These values are used to compare the void ratio values, which indicate the pore spaces in the samples from different depths under different situations. The initial void ratio values of the air dried samples were almost three times higher then the initial void ratio values (minimum stress applied was 0 kPa) of the undisturbed samples, where as the final void ratio values (maximum stress applied at 2500 kPa) were about two times higher. In case of the disturbed dry and saturated samples, we observe that the values of the mean void ratios decrease with the increase of stresses in both of the samples from 4 m and 8 m depths. When the values of the mean void ratios are compared with that of the undisturbed and the disturbed dry samples, they were always in between the undisturbed and the disturbed dry samples.

Table 3. Mean initial (at 0 kPa stress) and final void ratio (at 2500 kPa stress) values of air dried and undisturbed samples

Depth (m)	Air Dried		Undisturbed	
	Initial	Final	Initial	Final
4	0.9366	0.4902	0.3478	0.2096
6	0.8286	0.4677	0.3925	0.2430
8	0.8865	0.4731	0.4188	0.2556
10	0.8012	0.4207	0.3404	0.2244

Table 4. Mean initial (at 0 kPa stress) and final void ratio (at 2500 kPa stress) values of rewetted samples from 4 m and 8 m depth

Stress (kPa)	Rewetted 4 m		Rewetted 8 m	
	Initial	Final	Initial	Final
0	0.7614	0.2849	0.6777	0.3553
5	0.5995	0.2861	0.5776	0.3284
10	0.6143	0.2940	0.5550	0.3357
20	0.5433	0.2823	0.5365	0.3131

The difference in the initial void ratios between the disturbed dry and disturbed dry and saturated samples also increases with the increase in the pre-load but the difference in the final void ratios was same. In case of the undisturbed samples the difference in the initial void ratios decreases with the increase in pre-load. We expected the final void ratios of the disturbed dry and saturated samples to be equal to that of the undisturbed samples. In our results we find that the disturbed wet curves were moving closer to the undisturbed curve but do not meet with the undisturbed curve. This can be due to the reason that the applied pre-load may not be sufficient and requires a higher pre-load. The maximum applied stress was 2500 kPa which is equal to the vertical effective stress at 130 m depth calculated based on the value of dry bulk density. Even though the samples were applied with so high stresses, we could not get the void ratio values equal to the void ratio values of undisturbed samples. This indicates that the samples need to be stressed more then the applied but if we consider the depths from which the samples were taken they were only from 4 m to 10 m deep and not from a depth of 130 m, which explains us that the glacial till has reached its ideal packing stage under natural conditions. Further this approves our assumption that the particles were ideally packed under natural conditions by sorting for example by lateral movements etc. We also have observed that after loading the samples in the oedometer up to 2500 kPa and when the loads were removed there was an expansion in the samples observed (void ratio values increase by about 0.02), which can be due to the elasticity in the particles. So we infer that even after unloading up to 2500 kPa there is still elastic behaviour of the soil which indicates that to get the values comparable to the pre-cut section, the stress must be much higher then that of the natural conditions.

5.3 Water-induced compaction under disturbed dry and saturated conditions

Figure 26 shows the values of the pre-consolidation load of the samples from 4 m depth, which were pre-loaded with different stresses. With respect to the assumption that water induced compaction causes a plastic deformation. We expected to find these values comparable to the applied loads during saturation. The dashed line represents the expected effective stress depending on the pre-load applied on the samples. The values obtained were more then the expected values, however they were near to the expected values except in the case of sample one and sample two does not show any comparison.

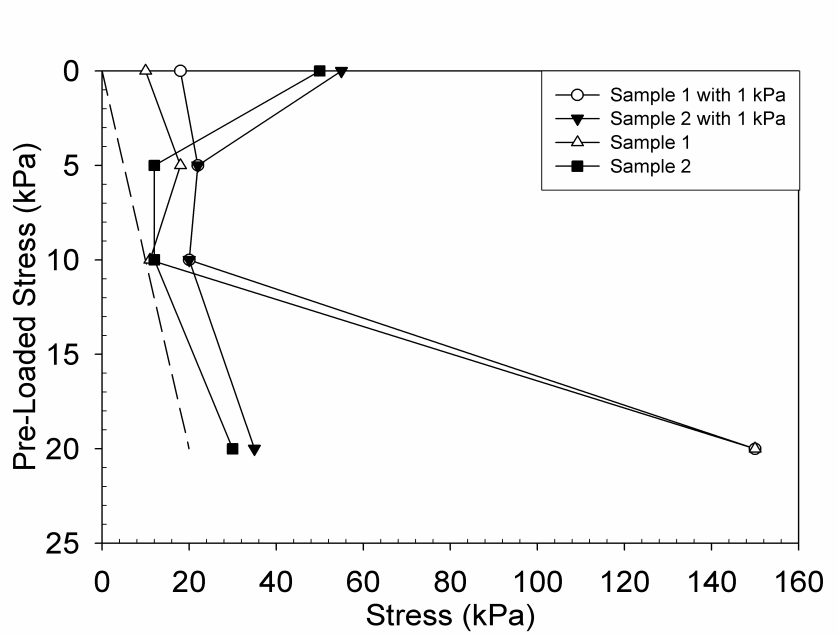

Figure 26. *Pre-consolidation load under disturbed dry and saturated conditions. 2 replicates from 4 m depth considering the void ratio value at 1 kPa and without.*

Figure 27 shows the values of the pre-consolidation load of samples from 8 m depth. The values obtained were more then the expected values, but were a bit realistic as the values obtained were near to the expected value until 10 kPa. The trend shows that when the samples were pre-loaded with 20 kPa the pre-consolidation value decreased.

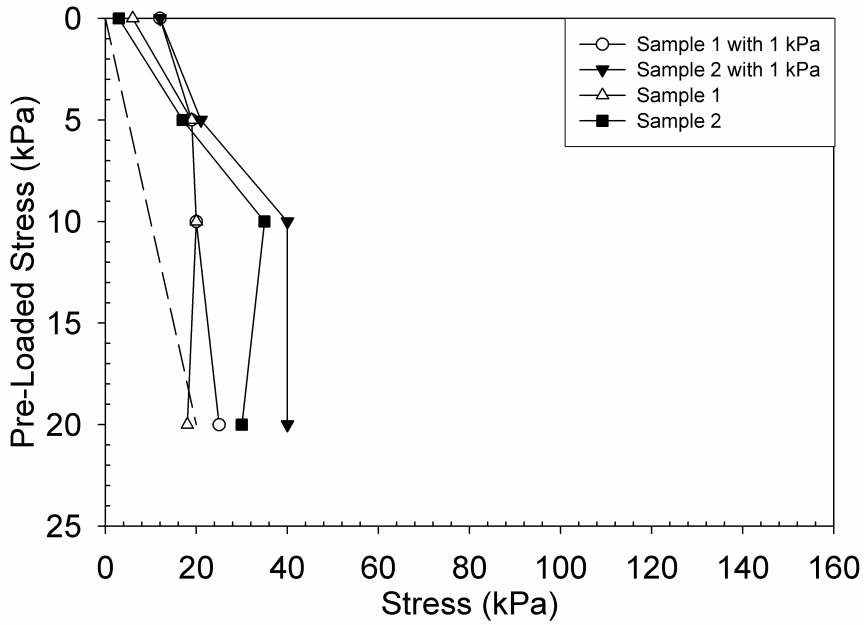

Figure 27. *Pre-consolidation load under disturbed dry and saturated conditions. 2 replicates from 8 m depth considering the void ratio value at 1 kPa and without.*

This can be due to the overestimation by the casagrande graphical method. It is subjective to find the pre-consolidation load values based on the casagrande graphical method. As it is difficult to find out the point where the radius of curvature is minimum and also in the case of virgin compression line. Another reason would be the accuracy in the oedometer apparatus. As the oedometer apparatus was not a completely fixed one, every time we had to fix the dial gauge on top of the plate and in some cases the dial gauge did not give the readings when the settlement observed was more. There might be also an error while placing the weights in the oedometer.

5.4 Changes in stress-strain behaviour due to water-induced compaction simulated for different depths (loads)

This was done for two depths 4 m and 8 m. Figure 28 shows the consolidation curves of the samples of undisturbed, disturbed dry, disturbed wet with different stresses from 4 m depth. The curves were fitted using the Equation [7] considering the value at 1 kPa stress. We also observe that the final void ratio of all the disturbed wet curves is almost the same value. We observe that with the increase in the stress the curves get closer to each other and assume a flatter shape similar to the shape of the curve obtained by undisturbed sample. The difference between the void ratio values of the disturbed dry and the disturbed wet curves gives the magnitude of the hydro-collapse.

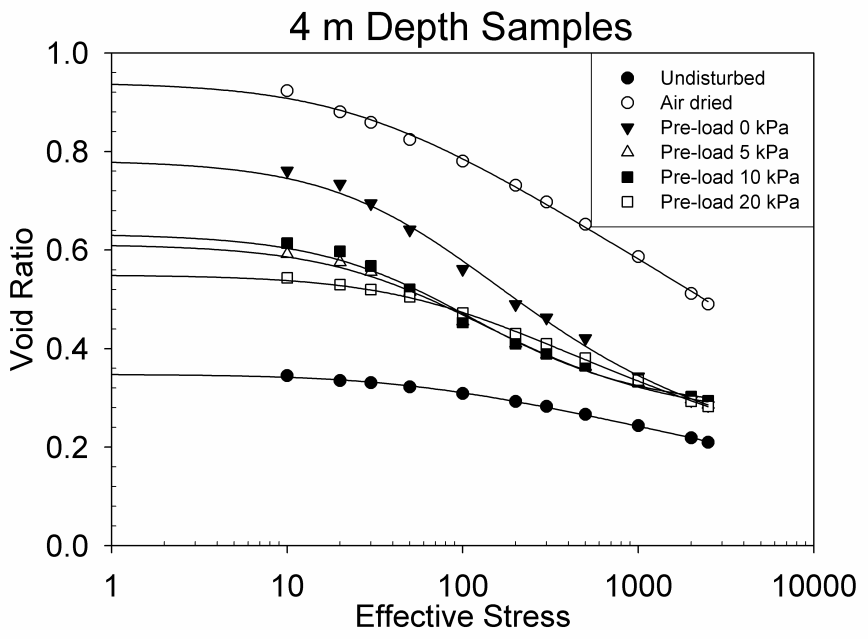

Figure 28. Curves plotted of undisturbed, disturbed dry, disturbed wet samples from 4 m depth.

Figure 29 shows the consolidation curves of undisturbed, disturbed dry, disturbed wet with different stresses from 8 m depth. The mean void ratio values of the disturbed wet samples lie in between the undisturbed and the disturbed dry samples. Here also we observe that as the stress was increased from 0 kPa to the 20 kPa the curves get closer and become flatter. The difference between the initial void ratio and the final void ratio values where less in the case of 8 m samples compared to that of 4 m samples.

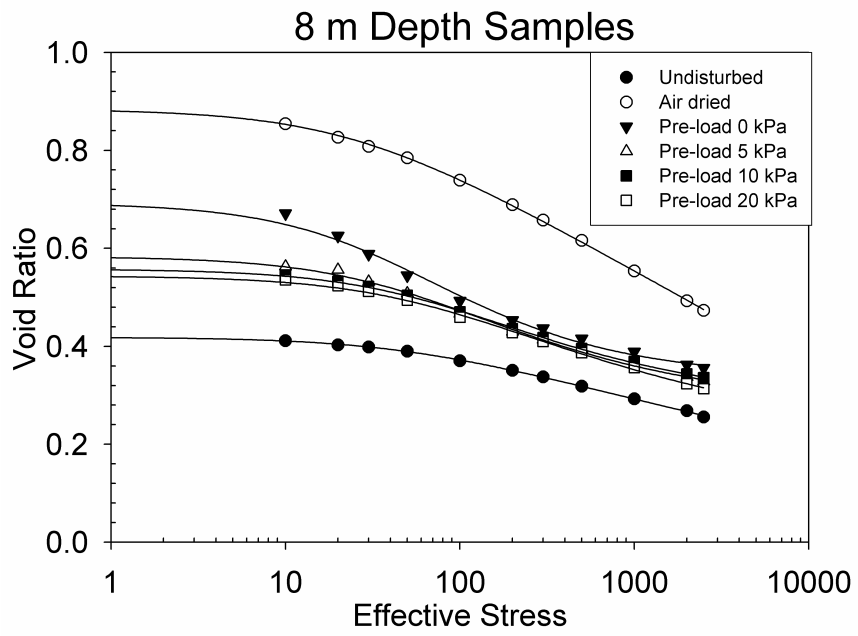

Figure 29. Curves plotted of undisturbed, disturbed dry, disturbed wet samples from 8 m depth.

We also observe from the Figure 28 and Figure 29 that there is a decrease in the void ratio values with the increase in the pre-loads of the disturbed wet samples. This decrease in the void ratios was logarithmic and not linear as the difference between the void ratio values observed from step 1 (0 kPa) and step 2 (5 kPa) stresses differs from the difference between the values in step 2, step 3 (10 kPa) and step 4 (20 kPa) stresses applied. The disturbed wet curve pre-loaded with step 4 stress has a similar shape as that of the undisturbed samples. This indicates that the disturbed dry and saturated samples are taking the shape of the undisturbed curve with increasing pre-loads. So we tried to find out the value at which the initial void ratio value of the disturbed wet curve will be same as that of the initial void ratio value of the undisturbed curve. The stress required was 900 kPa in the case of 4 m samples and 600 kPa for 8 m samples. The undisturbed samples were taken from the pre-cut section which is with out any external load acting over it but still we see that the soil particles are ideally packed which can be due to the oscillation of the glacial till under ice glaciation.

5.5 Modeling of pre-consolidation stress curves

At stresses smaller than the pre-consolidation load the soil is essentially elasto-plastic and not purely elastic i.e. the stress values below the pre-consolidation load are not completely elastic and recoverable, as often assumed theoretically. This can be explained as the only one time elastic rebound after the relief of the strain at the point where the pre-consolidation is calculated (as explained by Casagrande). In the range of pure elastic, recoverable volume change is very small and it cannot be completely recovered. O'Sullivan & Robertson, (1996) suggested a soil compaction model which takes into account the fact that there is an irreversible volume change even if the applied stress was smaller than that of the pre-consolidation load. Figure 30 shows the rebound taking place along the recompression line (RCL). Recompression takes place along the RCL 1 until the so-called yield line is reached. Recompression then follows a steeper line, known as plastic recompression line or steeper recompression line, (RCL 2) until the virgin compression line (VCL) is reached. The model proposed with these three lines RCL 1, RCL 2 and VCL was a closer approximation to the real compaction curve compared with the commonly-used models with two lines only RCL and VCL.

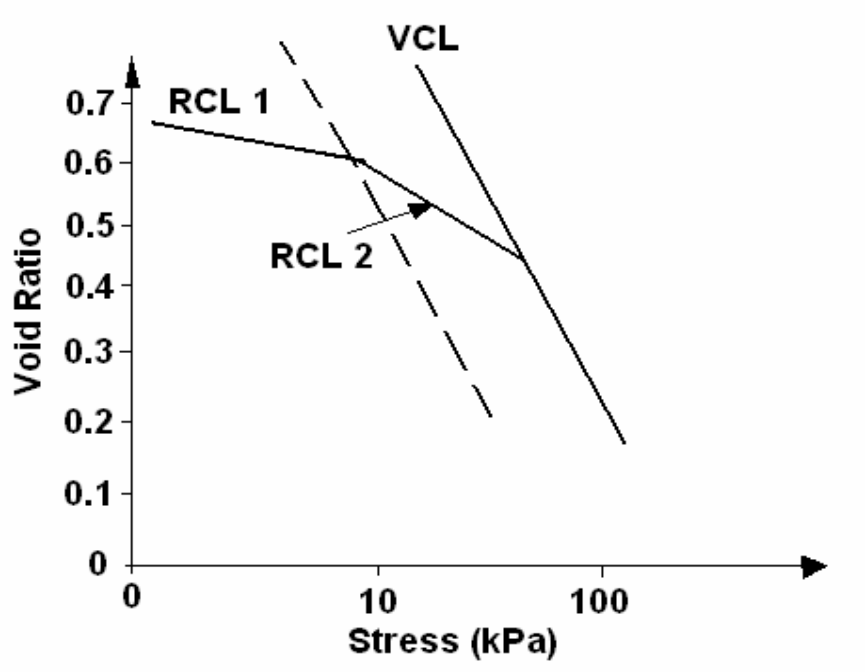

Figure 30. Soil compaction model as proposed by O'Sullivan & Robertson. (1996).

The void ratio values obtained from the oedometer test for the samples for respective stresses were plotted in the form of graphs. Then the curves were fitted using the modified van Genuchten equation [7]. In the beginning we tried to fit the curves for the best fit, in which we did not give any limiting constraints, i.e. the curves were freely fitted. In the second case we gave a constraint for the maximum void ratio value, in which we substituted the value of the maximum void ratio directly in the equation. The data were fitted with the equation [7] and the pre-consolidation load was calculated graphically using casagrande 1936 method. The fitted graphs are shown in the Appendix 9 for the undisturbed samples. The disturbed dry samples and the disturbed wet sample graphs are shown in Appendix 10 and Appendix 11 respectively. While fitting the curves with equation [7] we also tried to model the pre-consolidation load using the void ratio value at the 1 kPa load and also without, as we had a doubt that there will be a shift in the pre-consolidation load at the void ratio value of 10 kPa stress when we consider the value at 1 kPa, which was clearly observed in some samples. This is because the values of the void ratio values at 0 kPa were less high at the stresses of 10 kPa with respect to O'Sullivan & Robertson. (1996), indicating that there is not much of consolidation happening till the 10 kPa load (Figure 31). We also observed that the values obtained in our observations that the curves have three lines as explained by O'Sullivan & Robertson. (1996), the dashed line represents the yield line.

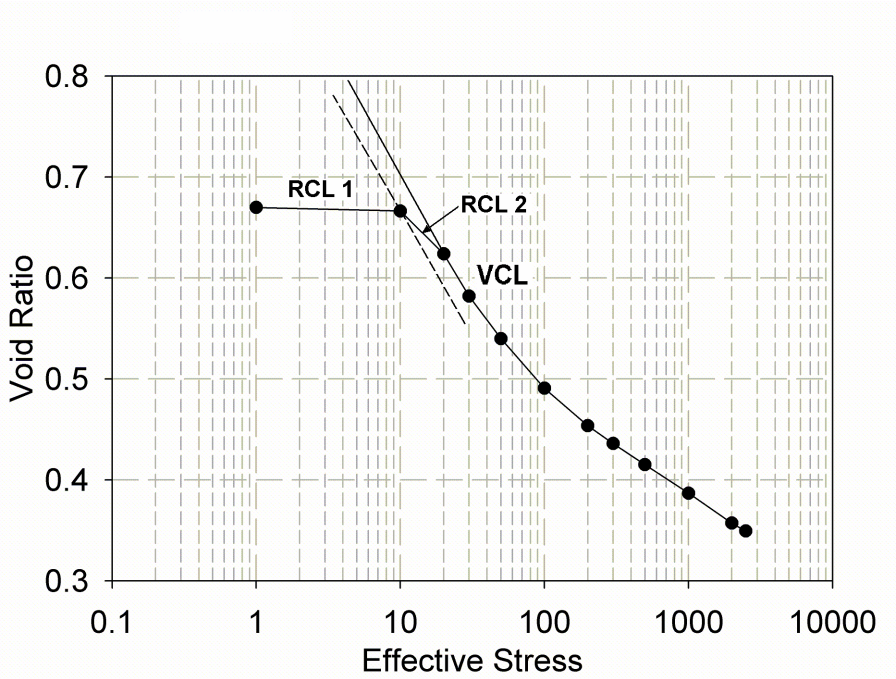

Figure 31. Modeling of pre-consolidation load using the void ratio value in comparison with O'Sullivan & Robertson, (1996) model. (8 m rewetted with 0 kPa pre-load)

Another problem which became evident was fitting of the curves. Figure 30 shows the curves which were best fitted with out any constraints of the maximum void ratio and also the curve best fitted with the maximum void ratio constraint. The graphs drawn in the case of undisturbed and the disturbed dry samples did not show any difference in the initial void ratio values whether they were fitted with the constraint of maximum void ratio or not. But on contrary in the graphs of the rewetted samples we find a huge difference in the initial void ratio values with the constraint and with out constraint.

In Figure 32 the curve which has the initial void ratio value of 0.67 is fitted with the constraint maximum void ratio value and we see that the curve does not fit all the value obtained. The second curve which has an initial void ratio of almost equal to 0.8 is freely fitted without any constraint but the maximum value of the initial void ratio obtained was only 0.67. This second curve though fits all the values obtained it overestimates the initial void ratio value. This means that the value of the pre-consolidation load is shifted towards the left side. This is due to the reason that there is no significant change in the void ratio values until 10 kPa stress applied in the oedometer as the values obtained at 0 kPa and 10 kPa were almost equal. The curve fit could not fit all the points when the constraint of the maximum (initial) void ratio value was given, which can be due to the reason that curve fit equation is designed as a sigmoidal function (classical S-curve). So the three line method given by O'Sullivan & Robertson, (1996) is considered as the better solution for finding out pre-consolidation values.

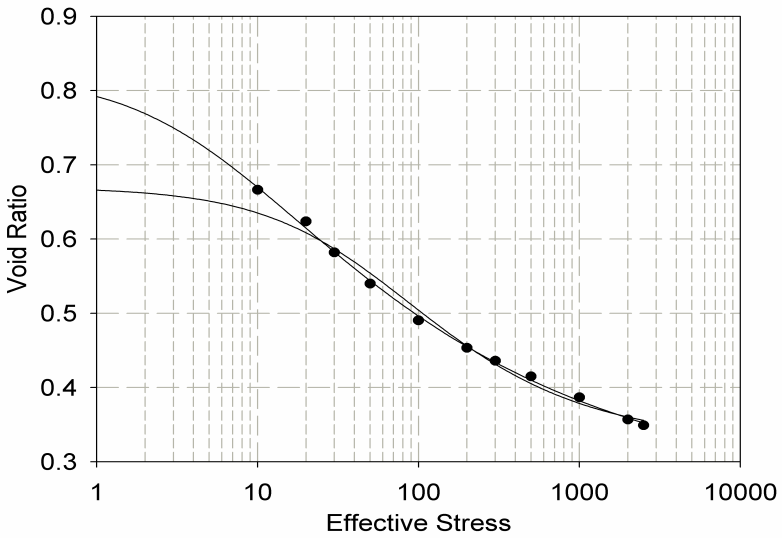

Figure 32. Showing the fitted curves with the constraint of the maximum void ratio and the curve freely fitted. (8 m rewetted with 0 kPa pre-load)

6. Conclusion

The **pre-consolidation loads with depth at the pre-cut section under natural conditions** (undisturbed condition) were in the range of 40 and 90 kPa. The obtained values were less then the expected values. We also observe that there is a shifting of the curve towards left and the difference between the value obtained and the expected values was increasing with the depth. On basis of the engineering science which can be explained as the shift in the stress caused by external concentrated loading.

The **effects of water-induced compaction on void ratio** showed different results: i) The average initial void ratio values of the disturbed dry samples were three times higher then the initial void ratio values (recorded at stress 0 kPa) of the undisturbed samples, where as the mean final void ratio values (recorded at stress 2500 kPa) were two times higher. In case of the disturbed wet samples, we observe that the values of the average initial void ratio values decrease with the increase in pre-loads.

ii) Pre-consolidation loads of the disturbed wet samples were in the range of 10 to 150 kPa for the samples from 4 m depths with different pre-loads where as the samples from the 8 m depth were in the range of 3 to 40 kPa which have showed realistic values. These results show that there is an increase in the pre-consolidation load value with the increase in the pre-load values. All the values obtained were above the vertical effective stress line as expected based on the pre-loads applied indicating over-consolidation.

iii) Modelling of water induced compaction depending on the various operations carried out in the mining field was analysed. Disturbed dry condition representing the transport of soil on the conveyor belt after the tillage and the disturbed wet conditions representing the situation, when there is increase in the water level and the overlying soil acts as the overburden. The magnitude of the collapse is known by the difference in the void ratio values of the disturbed dry and the disturbed wet samples. Even though the disturbed wet samples had different initial void ratio values the final void ratio values were same. The difference between the initial void ratio a final void ratio values of disturbed dry and disturbed wet samples from 4 m were greater then that of the samples from 8 m depth. We observed a collapse when the dry samples were wetted and loaded and the intensity of the collapse reduces with the increase in the stress values. The collapse has increased with the increase in the applied pre-loads and the magnitude of the collapse has decreased with increase in depth.

In the **modelling of pre-consolidation load,** we found out that there was an overestimation of the void ratio value when the curves were freely fitted with out any constraint of the maximum void ratio but the pre-consolidation loads calculated were realistic. On contrary when the curves were fitted with the constraint of the maximum void ratio value then the point at which the radius of curvature was minimum got shifted to the left of the curve.

7. Summary

The objective of this thesis work was to understand and model the water induced consolidation process at agriculturally used reclaimed soils. The approach was to reproduce the situation occurring when the soil was subjected to water induced compaction at defined loads typical in the top soil (0 kPa, 5 kPa, 10 kPa and 20 kPa).

The glacial till used for the experiments was sampled in the Lusatian lignite-mining district located about 100 km southeast of Berlin, Germany. The glacial till used for the experiments derived from the sediment layer of Warthe sub-stage of the saalian glaciation. To have an idea on the soil characteristics at the pre-cut section, parameters like grain size distribution, soil bulk density, calcium carbonate content ($CaCo_3$) and water retention characteristics were measured.

The stability of the glacial till was evaluated using pre-consolidation loads. This was done in three sub-steps. The first step was to determine the stress-strain behaviour under natural conditions. In the second step, stress-strain behaviour of disturbed dry samples was simulated, which would be the situation in summer when the glacial till dries during transport. In the third step we saturated the disturbed dry samples with different pre-loads, which simulate the effect of saturation and re-compaction by precipitation. This work on different samples is carried out with the help of uniaxial compression tests.

This work was exemplarily done for undisturbed samples and also for disturbed dry samples from 4 depths (4 m, 6 m, 8 m, and 10 m). The disturbed dry and saturated samples with certain pre-loads were tested at depths of 4 m and 8 m. Sediment samples for the different investigations were taken from the pre-cut section of the glacial high terrace ‘Hornoer Berg’ from a depth of 3 m to 10 m depth.

The glacial till has been classified as loamy sand (USDA soil texture classification). From the results of the grain size distribution it is seen that the soil particles were uniformly distributed with soil particles of different sizes indicating intermixture of the particles. High soil bulk density was recorded, which were in the range of 1.9 g cm^{-3} to 2.0 g cm^{-3} indicating that the profile to be compacted glacial till (Brady *et al.,* 2002). From the water retention characteristics we observe that the samples from 4 m and 10 m depth do not have coarse pores as the drainage of the samples started from the point above field capacity and were opposite in the case of samples from 6 m and 8 m depths.

On the basis of the carbonate content, the profile could be divided into two layers, top layer containing no carbonate and the deeper layer having carbonate content up to 5.4%.

The graphs obtained from the undisturbed samples showed a flat curve having the initial void ratio and final void ratio values in between 0.2 and 0.4. The pre-consolidation stress values obtained were in between 40 and 90 kPa, where as in the case of the disturbed dry samples the curves showed a huge difference in the value of the initial and final void ratio values. When the samples were saturated with different pre-loads the difference in the initial void ratio was decreasing while the final void ratio was same for all the curves. The trend for the pre-consolidation loads obtained was in the same range for undisturbed samples and disturbed wet samples, where as in case of the disturbed dry samples there was a decreasing trend observed with respect to depth.

We find that the magnitude of water induced compaction increased with the increase in pre-loads and a decrease with respect to the depths.

8. References

Alawaji H.A, 2001. shear induced collapse settlement of arid soils

Assalay.A.M, Jefferson.I, Ragers.C.D.F, Smalley.I.J, 1997. Fragipan formation in loess soils: development of the Bryant hydroconsolidation hypothesis.

Assouline. S, 2002. Modelling soil compaction under uniaxial compression.

Badawy S I.F, Hussain M.A, 2004. Effect of starting material particle size on its agglomeration behaviour in high shear wet granulation.

Barsh H and Billwitz K, 1990. Physisch-Geographische Arbeitsmethoden. 1. Auflage, Haack, Gothe.

Baumgartl. Th, 1998. Physical soil properties in specific fields of application especially in anthropogenic soils.

Baumgartl Th, 2002. The dynamic of water retention curves caused by soil deformation.

Baumgartl. Th, Köck. B, 2004. Modelling volume change and mechanical properties with hydraulic models.

Bodman G.B, Constantin G.K, 1965. Influence of particle size distribution in soil compaction.

Brandy.N.C, Well.R.R, 2002. The nature and properties of soils.

Brückmann W, Moran K and MacKillop A.K, 1997. Permeability and consolidation characteristics from hole 949B, northern Barbados ridge, GEOMAR Research Center Marine Geosciences, Kiel, Federal Republic of Germany.

Brye.K.R, 2003. Long-term effects of cultivation on particle size and water-retention characteristics determined using wetting curves.

Carter.M.R, 1993. Soil sampling and methods of analysis.

Casagrande.A, The determination of pre-consolidation load and its practical significance.

Clementino R.V, 2005. Discussion of "An oedometer test study on the pre-consolidation stress of glaciomarine clays

Constantini E.A.C, Damiani. D, 2004. Clay minerals and the development of quarternary soils in central italy.

Dexter A.R, Horn.R, Kempert.W.D, 1988. Two mechanisms for age-hardening of soil.

Dexter A.R, Birkas M, 2004. Predistion of the soil structures produced by tillage.

Dibben.S.C, Jefferson.I.F, and Smalley.I.J, The Loughborough Loess : Monte carlo model of soil.

Dijkstra T.A, Smalley I.J, Rogers C.D.F, 1995. Particle packing in loess deposits and the problem of structure collapse and hydroconsolidation

Dirksen.C, 1999. Soil physics measurements.

Ford. E.J. 1997. Soil water retention determination using the 'wetlab' facility at CSIRO, Davies laboratory.

Fredlund.M.D, Sillers.W.S, Fredlund.D.G, Wilson.G:W, Design of a knowledge-based system for unsaturated soil properties.

Fredlund M.D, Fredlund.D.G, Wilson.G.W, Prediction of the soil-water characteristic curve from Grain-size distribution and volume-mass properties.

Fritton.D.D, 2001. An improved empirical equation for uniaxial soil compression for a wide range of applied stresses.

Froehlich HA, McNabb DH , 1984. Minimizing soil compaction in Pacific Northwest forests. In Forest Soils and Treatment Impacts.

Greacen E.L, 1960. Water content and soil strength.

Haiquan Zhang, Hratge.K.H and Ringe H, 1997. Effectiveness of organic matter incorporation in reducing soil compactibility.

Hartmann C, Poss.R, Janeau.Jean-Louis, Bourdon.E, Lesturgez.G, Ratana Anupap.S, 2002 Use of the granular material theory to interpret structural changes in a sandy soil.

Horn.R, Albrechts.C, Stress-Strain dependent changes of soil structure in arable and forest soils – consequences for the environment.

Jakob H.Dane, Clarke top.G, Methods of soil analysis part-4: Physical methods.

Jefferson.I.F, Smalley.I.J, Saltating sand erodes metastable loess: events in the inpact zone.

John Williams and shaykewich C.F, 1970. The influence of soil water metric potential on strength properties of unsaturated soil.

Klute.A, 1986. Methods of soil analysis: Physical and mineralogical methods.

Laberg J.S, Vorren T.O, 2000. The Trñnadjupet Slide, offshore Norway Ð morphology, evacuation and triggering mechanisms

Lebert. M and Horn.R. Prediction of mechanical strength of soil.

Lebert. M and Horn.R, 1991. A method to predict the mechanical strength of agricultural soils.

Lesturgez Gregory, Daniel Tessier, Elliane Huard, Hartmann.C, and Poss.R, 2004. Collapsing and traffic load: the formation of dense layer in a sandy soil.

Miller H, Djerbib Y, Jefferson I.F and Smalley I.J, 1998. Modelling the Collapse of Metastable Loess Soils

Mullins.C.E, Macleod.D.A, Northcote.K.H, Tisdall.J.M, Young.I.M, 1990. Hardsetting Soils: Behaviour, occurrence, and management.

Park S.J, P. Almond, K. Mc Sweeney, and B. Lowery, 2002. Fragipan formation within closed depressions in southern Wisconsin.

Radka Kodesova, 2003. Percolation theory and its application interpretation of soil water retention curves.

Rampino. C, Claudio Mancuso, and Filippo Vinale, 2000. Experimental behaviour and modelling of an unsaturated compacted soil

Sclichting E., Blume H.P and K. Stahr, 1995. Bodenkundliches praktikum 2. Auflage, Blackwell Berlin.

Semmel. H, Horn.R, Hell.U, Dexter A.R, Schulze.E.D. 1990. The dynamics of soil aggregate formation and the effect on soil physical properties.

Shehata W.M, Amin A.A, 1997. Geotechnical hazards associated with desert environment

Skempton A.W. Effective stress in soils, concrete and rocks.

Silva A.J, 1996. Seabed Slopes Processes in Deep Water Continental Margin, Northwest Gulf of Mexico

Smith.K.A, Mullins.C.E, 1991. Soil analysis: Physical methods.

Snyder and Miller, 1985. Tensile strength of unsaturated soils.

Stock.O, Grünewald.H, Bens.O, Hüttl.R.F., 2004, High Bulk Density of reclaimed post-mining soils-A result of reconsolidation.

Stock.O, Lesturgez.G, Bens.O, Hüttl.R.F, 2005. Untersuchungen zum Verfestigungsverhalten saalezeitlichen Geschiebemergels am Beispiel Landwirtshaftlicher Rekultivierungsstandorte der Niederlausitzer Bergbaufolgelandschaft. Ph.D. Thesis.

Unger P.W, 1995. Soil bulk density, penetration resistance, and hydraulic conductivity under controlled traffic conditions.

Van Genuchten M.Th 1980. A closed form equation for predicting the hydraulic conductivity of unsaturated soils.

Vrolijk P,Miller T, and Gooch M.J, 1998. hydrostatic consolidation tests of undeformed, clay-rich samples from the Barbados accretionary prism, LEG 156.

Zhang.B, Zhao.Q.G, Horn.R, Baumgartl.T, 2000. Shear strength of surface soil as affected by soil bulk density and soil water content.

Zhuang Ying-chun, Xie Kang-he, Li Xi-bin, 2004. Nonlinear analysis of consolidation with variable compressibility and permeability.

Appendix 1

Table 5. Grain Size Distribution

Profile	Depth [cm]	> 2 mm [%]	> 1 mm [%]	> 0,5 mm [%]	>0,25 mm [%]	> 0,125 mm [%]	> 0,063 mm [%]	> 0,020 mm [%]	> 0,006 mm [%]	> 0,002 mm [%]	< 0,002 mm [%]	S [%]	U [%]	T [%]
A-4	400	3.2	2.7	8.8	17.9	20.4	15.2	4.4	11.0	-0.7	17.0	68.3	14.8	17.0
B-4	400	3.0	3.2	9.2	17.8	20.5	15.2	8.9	11.2	5.9	5.1	68.9	26.0	5.1
C-4	400	3.0	2.6	9.1	18.0	20.6	14.7	10.1	11.9	5.2	4.7	68.1	27.2	4.7
Average		3.1	2.9	9.1	17.9	20.5	15.0	7.8	11.4	3.5	8.9	68.4	22.6	8.9
		100.0	96.9	94.1	85.0	67.1	46.6	31.6	23.8	12.4	8.9			
A-6	600	0.9	2.4	8.4	16.9	22.5	18.4	3.0	12.9	6.0	8.6	69.5	22.0	8.6
B-6	600	1.6	2.5	8.3	16.8	22.1	17.8	10.4	12.4	4.7	3.4	69.2	27.4	3.4
C-6	600	1.6	2.8	8.0	16.5	21.8	17.2	10.6	12.1	5.2	4.0	68.0	28.0	4.0
Average		1.4	2.6	8.3	16.7	22.2	17.8	8.0	12.5	5.3	5.3	68.9	25.8	5.3
		100.0	98.6	96.1	87.8	71.1	48.9	31.1	23.1	10.6	5.3			
A-8	800	1.3	1.8	6.5	14.3	21.4	20.0	-6.4	36.9	-6.7	10.9	65.3	23.8	10.9
B-8	800	1.4	2.0	6.9	14.5	23.0	19.4	9.7	12.3	5.6	5.3	67.2	27.6	5.3
C-8	800	0.9	1.7	6.7	14.8	21.3	19.6	14.1	12.2	5.0	3.7	65.0	31.3	3.7
Average		1.2	1.8	6.7	14.5	21.9	19.7	5.8	20.5	1.3	6.6	65.8	27.6	6.6
		100.0	98.8	96.9	90.3	75.7	53.8	34.2	28.4	7.9	6.6			
A-10	1000	1.3	2.0	7.2	15.3	21.0	17.1	2.9	11.4	14.1	7.6	63.9	28.5	7.6
B-10	1000	2.8	2.4	7.0	15.1	21.0	17.5	9.8	12.9	6.2	5.3	65.7	28.9	5.3
C-10	1000	1.7	2.5	7.6	16.0	21.6	17.7	14.0	10.8	4.8	3.2	67.1	29.6	3.2
Average		2.0	2.3	7.3	15.5	21.2	17.4	8.9	11.7	8.4	5.4	65.6	29.0	5.4
		100.0	98.0	95.8	88.5	73.0	51.8	34.4	25.5	13.8	5.4			

Table 6. Grain Size Distribution with Natrium Phosphate in the sedimentation process

Profil	Tiefe	> 2 mm	> 1 mm	> 0,5 mm	>0,25 mm	> 0,125 mm	> 0,063 mm	> 0,020 mm	> 0,006 mm	> 0,002 mm	< 0,002 mm	S	U	T
	[cm]	[%]	[%]	[%]	[%]	[%]	[%]	[%]	[%]	[%]	[%]	[%]	[%]	[%]
A-4	400	3.2	2.7	8.8	17.9	20.4	15.2	6.3	12.8	3.1	9.5	68.3	22.2	9.5
B-4	400	3.0	3.2	9.2	17.8	20.5	15.2	4.7	13.5	3.1	9.8	68.9	21.3	9.8
C-4	400	3.0	2.6	9.1	18.0	20.6	14.7	5.7	13.5	3.0	9.7	68.1	22.2	9.7
Average		3.1	2.7	9.0	18.0	20.5	15.0	6.0	13.1	3.1	9.6	68.2	22.2	9.6
		100.0	96.9	94.2	85.3	67.3	46.8	31.8	25.8	12.7	9.6			
A-6	600	0.9	2.4	8.4	16.9	22.5	18.4	5.8	12.7	3.0	9.0	69.5	21.6	9.0
B-6	600	1.6	2.5	8.3	16.8	22.1	17.8	7.1	12.5	2.5	8.7	69.2	22.2	8.7
C-6	600	1.6	2.8	8.0	16.5	21.8	17.2	5.9	14.1	2.4	9.7	68.0	22.3	9.7
Average		1.2	2.6	8.2	16.7	22.2	17.8	5.9	13.4	2.7	9.3	68.7	22.0	9.3
		100.0	98.8	96.2	88.0	71.3	49.1	31.3	25.4	12.0	9.3			
A-8	800	1.3	1.8	6.5	14.3	21.4	20.0	6.9	14.5	3.4	10.0	65.3	24.7	10.0
B-8	800	1.4	2.0	6.9	14.5	23.0	19.4	5.9	14.5	2.9	9.5	67.2	23.3	9.5
C-8	800	0.9	1.7	6.7	14.8	21.3	19.6	12.0	12.7	2.8	7.5	65.0	27.5	7.5
Average		1.1	1.8	6.6	14.5	21.3	19.8	9.4	13.6	3.1	8.7	65.1	26.1	8.7
		100.0	98.9	97.1	90.5	76.0	54.7	34.9	25.4	11.9	8.7			
A-10	1000	1.3	2.0	7.2	15.3	21.0	17.1	6.6	16.6	2.4	10.5	63.9	25.6	10.5
B-10	1000	2.8	2.4	7.0	15.1	21.0	17.5	4.6	16.6	2.8	10.3	65.7	24.0	10.3
C-10	1000	1.7	2.5	7.6	16.0	21.6	17.7	10.4	11.5	3.3	7.7	67.1	25.2	7.7
Average		1.5	2.2	7.4	15.7	21.3	17.4	8.5	14.1	2.8	9.1	65.5	25.4	9.1
		100.0	98.5	96.3	88.8	73.2	51.9	34.5	26.0	11.9	9.1			

Appendix 2

Table 7. Soil Bulk Density and water content

Sample depth [cm]	Bulk density (mean) g/cm³	Water content (mean) cm³/cm³
300	1.892	0,164
400	2.016	0,23
500	1.958	0,194
600	1.932	0,2
700	1.856	0,196
800	1.888	0,93
900	1.994	0,226
1000	2.008	0,298

Appendix 3

Table 8. Carbonate Content

Sample	Weight (g)	Room temp. (°C)	Air pressure (hPa)	Start (ml)	End (ml)	Carbonate %
(I) 4-m	4,0843	21,5	1016	27,4	28,2	0,1
(II) 4-m	5,6598	21,5	1016	25,0	26,2	0,1
(III) 4-m	5,1992	21,5	1016	23,4	24,8	0,1
(I) 6-m	3,5639	21,5	1016	24,4	24,8	0,0
(II) 6-m	4,3702	21,5	1016	23,8	25,0	0,1
(III) 6-m	5,8121	21,5	1016	23,4	24,2	0,1
(I) 8-m	4,2069	21,5	1016	23,8	74,8	5,0
(II) 8-m	5,4448	21,5	1016	23,4	98,6	5,7
(III) 8-m	5,0918	21,5	1016	24,0	88,6	5,3
(I) 10-m	3,4091	21,5	1016	20,8	63,2	5,2
(II) 10-m	5,2535	21,5	1016	22,3	97,2	5,9
(III) 10-m	5,6265	21,5	1016	23,6	92,4	5,1

Appendix 4

Table 9. Water Retention Curves (pF-Curves)

Height (cm)	Sample No.	Weight of sample (Fresh)	Weight of sample (10hpa)	Weight of sample ($10^{1.5}$hpa)	Weight of sample ($10^{1.8}$hpa)	Weight of sample (10^{2}hpa)	Weight of sample ($10^{2.3}$hpa)	Weight of sample ($10^{2.5}$hpa)	Weight of sample ($10^{2.8}$hpa)	weight of sample (10^{3}hPa)		weight of sample ($10^{4.2}$hPa)	
400		21.677	23.037	22.727	22.747	21.857	20.217	18.647	18.157	17.4	16.88235	8.705882	8.352941
		22.229	24.429	23.769	23.139	22.519	20.799	19.089	18.379	17.58824	15.77647	8.941176	8.352941
		21.517	24.947	23.427	23.247	22.057	20.267	18.387	17.687	16.78824	17.64706	8.352941	8.470588
		21.753	24.753	23.673	23.503	22.553	20.923	19.203	18.703	17.69412	16.61176	8.705882	8.705882
		21.276	24.326	23.586	22.716	22.186	20.356	18.406	17.766	16.22353	17.57647	7.764706	8.235294
600		20.82	25.42	23.62	21.2	19.24	17.25	15.93	15.42	13.32941	14.98824	5.882353	6.705882
		20.515	25.575	23.645	20.705	19.345	17.355	16.125	15.485	13.12941	13.45882	6.117647	5.882353
		20.472	26.332	24.492	21.182	19.782	17.642	16.072	15.482	13.76471	13.01176	6.117647	5.764706
		20.384	24.854	22.614	20.064	18.874	16.974	15.634	15.164	15.98824	13.78824	6.117647	0.823529
		20.205	24.605	23.155	20.115	18.655	17.285	15.335	15.065	13.62353	14.28235	5.529412	6.470588
800		18.982	30.212	25.632	22.422	20.732	17.302	15.192	14.582	13.18824	13.51765	5.411765	5.529412
		17.927	27.917	24.057	21.137	19.447	16.177	14.067	13.457	13.32941	13.57647	5.058824	4.705882
		18.344	29.154	24.434	22.924	19.794	16.544	14.234	13.724	0.823529	13.22353	5.294118	4.941176
		19.092	28.592	25.052	23.582	20.342	17.072	14.852	14.302	12.70588	12.04706	4.941176	4.705882
		19.52	30.26	27.15	23.14	21.18	17.88	15.53	14.97	12.95294	14.03529	5.058824	5.058824
900		23.388	27.738	24.888	23.078	21.958	19.538	17.118	16.548	14.45882	14.51765	-1.52941	5.411765
		23.814	28.104	24.854	23.784	22.364	20.294	17.964	17.264	14.02353	14.81176	5.647059	6
		23.8	27.42	25.22	23.47	22.23	20.07	17.91	17.13	14.91765	13.95294	6.235294	5.882353
		24.231	27.781	25.511	23.921	22.681	20.351	17.751	17.061	15.09412	14.52941	5.529412	1.058824
		23.301	27.501	23.781	21.831	20.891	19.291	17.651	17.111	13.74118	15.76471	5.647059	5.882353
1000		30.947	26.537	26.347	26.087	26.027	25.347	19.257	17.947	15.2	14.31765	6.235294	5.647059
		30.367	27.127	26.487	26.327	26.197	23.177	18.997	18.037	15.31765	15.90588	0.705882	5.882353
		28.607	25.287	24.547	24.337	24.187	22.527	19.127	17.677	14.35294	14.56471	5.647059	5.882353
		31.042	26.972	26.662	26.442	26.362	25.882	19.112	17.922	15.02353	16.16471	6.352941	6.117647
		32.004	28.254	27.794	27.534	27.164	23.844	19.794	18.854	28.47059	14.41176	5.647059	5.529412

Appendix 5

Table 10. 4 m Depth Undisturbed samples

Applied Stress	400 cm Depth Undisturbed			
	Sample 1		sample2	
	Bulk Density	Void Ratio	Bulk Density	Void Ratio
[kPa]	[g/cm³]	e	[g/cm³]	e
0	1,9293	0,3735	2,0044	0,3221
10	1,9341	0,3701	2,0084	0,3195
20	1,9459	0,3619	2,0257	0,3082
30	1,9518	0,3578	2,0339	0,3029
50	1,9637	0,3495	2,0463	0,295
100	1,9849	0,3351	2,0664	0,2824
200	2,0139	0,3159	2,0879	0,2692
300	2,0319	0,3042	2,101	0,2613
500	2,0634	0,2843	2,1222	0,2487
1000	2,1074	0,2575	2,1553	0,2296
2000	2,1545	0,23	2,1942	0,2077
2500	2,172	0,2201	2,2099	0,1991

Table 11. 6 m Depth Undisturbed samples

Applied Stress	600 cm Depth Undisturbed			
	Sample 1		sample 2	
	Bulk Density	Void Ratio	Bulk Density	Void Ratio
[kPa]	[g/cm³]	e	[g/cm³]	e
0	1,9134	0,3849	1,8929	0,4
10	1,9134	0,3849	1,8976	0,3965
20	1,9298	0,3732	1,912	0,386
30	1,9367	0,3683	1,9198	0,3804
50	1,9505	0,3586	1,9305	0,3727
100	1,9706	0,3448	1,9514	0,358
200	1,9953	0,3282	1,9769	0,3405
300	2,012	0,3171	1,9946	0,3286
500	2,0377	0,3005	2,0234	0,3097
1000	2,0798	0,2741	2,0631	0,2845
2000	2,1249	0,2471	2,1056	0,2586
2500	2,1433	0,2364	2,1209	0,2495

Table 12. 8 m Depth Undisturbed samples

Applied Stress	800 cm Depth Undisturbed			
	Sample 1		Sample 2	
	Bulk Density	Void Ratio	Bulk Density	Void Ratio
[kPa]	[g/cm³]	e	[g/cm³]	e
0	1,8723	0,4154	1,8633	0,4222
10	1,8865	0,4047	1,869	0,4179
20	1,8912	0,4012	1,8869	0,4044
30	1,8931	0,3998	1,8965	0,3973
50	1,9028	0,3927	1,9111	0,3866
100	1,9282	0,3743	1,939	0,3667
200	1,9554	0,3552	1,9687	0,3461
300	1,9729	0,3432	1,9897	0,3319
500	2,0003	0,3248	2,0199	0,312
1000	2,0407	0,2986	2,0589	0,2871
2000	2,085	0,271	2,0936	0,2657
2500	2,1014	0,2611	2,1198	0,2501

Table 13. 10 m Depth Undisturbed samples

Applied Stress	1000 cm Depth Undisturbed			
	Sample 1		sample2	
	Bulk Density	Void Ratio	Bulk Density	Void Ratio
[kPa]	[g/cm³]	e	[g/cm³]	e
0	1,951	0,3583	2,0039	0,3224
10	1,952	0,3576	2,014	0,3158
20	1,9653	0,3484	2,0232	0,3098
30	1,9727	0,3433	2,0428	0,2973
50	1,9827	0,3365	2,0469	0,2946
100	2,001	0,3243	2,0638	0,284
200	2,0218	0,3107	2,0864	0,2702
300	2,0344	0,3026	2,0984	0,2629
500	2,0526	0,291	2,1139	0,2536
1000	2,0855	0,2707	2,1456	0,2351
2000	2,123	0,2482	2,1806	0,2153
2500	2,1334	0,2421	2,1961	0,2067

Appendix 6

Table 14. 4 m depth Disturbed Dry Samples

Applied Stress	400 cm Depth Disturbed Dry			
	Sample 1		sample2	
	Bulk Density	Void Ratio	Bulk Density	Void Ratio
[kPa]	[g/cm³]	e	[g/cm³]	e
0	1,3466	0,968	1,391	0,9051
10	1,3581	0,9512	1,3987	0,8946
20	1,3829	0,9163	1,4366	0,8446
30	1,4041	0,8873	1,4482	0,8299
50	1,4318	0,8509	1,4743	0,7975
100	1,4701	0,8027	1,507	0,7584
200	1,5147	0,7495	1,5468	0,7132
300	1,5451	0,7151	1,5771	0,6803
500	1,5917	0,6649	1,6165	0,6394
1000	1,6604	0,596	1,6804	0,577
2000	1,7431	0,5202	1,7624	0,5036
2500	1,7683	0,4986	1,7885	0,4817

Table 15. 6 m Depth Disturbed Dry Samples

Applied Stress	600 cm Depth Disturbed Dry			
	Sample 1		sample 2	
	Bulk Density	Void Ratio	Bulk Density	Void Ratio
[kPa]	[g/cm³]	e	[g/cm³]	e
0	1,4447	0,8343	1,4537	0,8229
10	1,4667	0,8068	1,4662	0,8074
20	1,4828	0,7871	1,4857	0,7837
30	1,4959	0,7715	1,5041	0,7618
50	1,5143	0,75	1,527	0,7354
100	1,5463	0,7137	1,5611	0,6976
200	1,5841	0,6729	1,5966	0,6597
300	1,6096	0,6463	1,6243	0,6315
500	1,6491	0,6069	1,6624	0,5941
1000	1,7086	0,5509	1,7235	0,5376
2000	1,7759	0,4922	1,7914	0,4793
2500	1,7968	0,4748	1,8143	0,4606

Table 16. 8 m Depth Disturbed Dry Samples

Applied Stress	800 cm Depth Disturbed Dry			
	Sample 1		Sample 2	
	Bulk Density	Void Ratio	Bulk Density	Void Ratio
[kPa]	[g/cm³]	e	[g/cm³]	e
0	1,4258	0,8586	1,3843	0,9143
10	1,4612	0,8136	1,3983	0,8952
20	1,4825	0,7875	1,4202	0,866
30	1,4988	0,768	1,4341	0,8478
50	1,5136	0,7508	1,4572	0,8186
100	1,5548	0,7044	1,4941	0,7736
200	1,6015	0,6547	1,5377	0,7234
300	1,6332	0,6226	1,5659	0,6923
500	1,6774	0,5798	1,6041	0,6521
1000	1,7457	0,518	1,6678	0,5889
2000	1,8163	0,459	1,7363	0,5262
2500	1,8409	0,4395	1,759	0,5066

Table 17. 10 m Depth Disturbed Dry Samples

Applied Stress	1000 cm Depth Disturbed dry			
	Sample 1		sample2	
	Bulk Density	Void Ratio	Bulk Density	Void Ratio
[kPa]	[g/cm³]	e	[g/cm³]	e
0	1,4698	0,803	1,4728	0,7993
10	1,5006	0,766	1,5059	0,7597
20	1,5215	0,7417	1,5294	0,7327
30	1,5391	0,7218	1,5536	0,7057
50	1,5649	0,6934	1,5803	0,6769
100	1,6002	0,656	1,6247	0,6311
200	1,6482	0,6078	1,6689	0,5879
300	1,6755	0,5817	1,6968	0,5618
500	1,7136	0,5465	1,7363	0,5262
1000	1,7708	0,4965	1,7928	0,4781
2000	1,8372	0,4424	1,8567	0,4273
2500	1,8564	0,4275	1,8744	0,4138

Appendix 7

Table 18. 4 m Depth Disturbed Dry and Saturated Samples with 0 kPa

Applied Stress	400 cm Depth Saturated with 0kpa			
	Sample 1		sample2	
	Bulk Density	Void Ratio	Bulk Density	Void Ratio
[kPa]	[g/cm³]	e	[g/cm³]	e
0	1,4994	0,7674	1,5096	0,7554
10	1,4994	0,7674	1,5115	0,7532
20	1,53	0,732	1,526	0,7365
30	1,5879	0,6688	1,5408	0,7198
50	1,673	0,584	1,5603	0,6983
100	1,7771	0,4912	1,625	0,6308
200	1,8505	0,432	1,7121	0,5478
300	1,8848	0,4059	1,7437	0,5197
500	1,9242	0,3772	1,8101	0,464
1000	2,0331	0,3034	1,9164	0,3828
2000	2,0603	0,2862	2,0325	0,3038
2500	2,0688	0,2809	2,056	0,2889

Table 19. 4 m Depth Disturbed Dry and Saturated Samples with 5 kPa

Applied Stress	400 cm Depth Saturated with 5kpa			
	Sample 1		sample 2	
	Bulk Density	Void Ratio	Bulk Density	Void Ratio
[kPa]	[g/cm³]	e	[g/cm³]	e
0	1,6673	0,5894	1,6465	0,6095
10	1,6786	0,5787	1,6519	0,6042
20	1,6987	0,56	1,6669	0,5898
30	1,7175	0,5429	1,69	0,568
50	1,7536	0,5111	1,7442	0,5193
100	1,8247	0,4523	1,8178	0,4578
200	1,8829	0,4074	1,8747	0,4135
300	1,9137	0,3848	1,9051	0,391
500	1,9472	0,3609	1,9411	0,3652
1000	1,9961	0,3276	1,9903	0,3314
2000	2,0426	0,2974	2,0441	0,2964
2500	2,0596	0,2866	2,0613	0,2856

Table 20. 4 m Depth Disturbed Dry and Saturated Samples with 10 kPa

Applied Stress	400 cm Depth Saturated with 10kpa			
	Sample 1		Sample 2	
	Bulk Density	Void Ratio	Bulk Density	Void Ratio
[kPa]	[g/cm³]	e	[g/cm³]	e
0	1,6075	0,6485	1,6729	0,58
10	1,6075	0,6485	1,678	0,5793
20	1,6139	0,6419	1,7071	0,5524
30	1,6542	0,602	1,7287	0,533
50	1,7142	0,5459	1,7731	0,4945
100	1,8001	0,4721	1,8475	0,4344
200	1,8509	0,4318	1,9097	0,3876
300	1,8763	0,4124	1,9408	0,3654
500	1,9035	0,3922	1,981	0,3377
1000	1,9461	0,3617	2,034	0,3029
2000	1,9858	0,3345	2,0873	0,2696
2500	1,9956	0,3279	2,103	0,2601

Table 21. 4 m Depth Disturbed dry and Saturated Samples with 20 kPa

Applied Stress	400 cm Depth Saturated with 20kpa			
	Sample 1		sample2	
	Bulk Density	Void Ratio	Bulk Density	Void Ratio
[kPa]	[g/cm³]	e	[g/cm³]	e
0	1,7209	0,5399	1,7135	0,5466
10	1,7209	0,5399	1,7135	0,5466
20	1,7269	0,5345	1,7382	0,5245
30	1,7335	0,5287	1,7542	0,5106
50	1,74	0,523	1,7825	0,4867
100	1,7574	0,5079	1,8449	0,4364
200	1,7893	0,481	1,9215	0,3792
300	1,8046	0,4684	1,9622	0,3506
500	1,8361	0,4433	2,0117	0,3173
1000	1,8947	0,3986	2,0826	0,2724
2000	1,9533	0,3566	2,1566	0,2288
2500	1,9645	0,349	2,18	0,2156

Appendix 8

Table 22. 8 m Depth Disturbed Dry and Saturated Samples with 0 kPa

Applied Stress	800 cm Depth Saturated with 0kpa			
	Sample 1		sample2	
	Bulk Density	Void Ratio	Bulk Density	Void Ratio
[kPa]	[g/cm³]	e	[g/cm³]	e
0	1,5721	0,6857	1,5872	0,6696
10	1,5816	0,6755	1,5904	0,6663
20	1,6283	0,6275	1,6321	0,6237
30	1,6618	0,5946	1,6752	0,5819
50	1,7107	0,5491	1,721	0,5398
100	1,7724	0,4952	1,7779	0,4905
200	1,8243	0,4526	1,8233	0,4535
300	1,8446	0,4366	1,8456	0,4359
500	1,871	0,4164	1,8728	0,415
1000	1,905	0,3911	1,9111	0,3866
2000	1,9379	0,3675	1,959	0,357
2500	1,9463	0,3616	1,9644	0,349

Table 23. 8 m Depth Disturbed Dry and Saturated Samples with 5 kPa

Applied Stress	800 cm Depth Saturated with 5kpa			
	Sample 1		sample 2	
	Bulk Density	Void Ratio	Bulk Density	Void Ratio
[kPa]	[g/cm³]	e	[g/cm³]	e
0	1,6732	0,5838	1,6865	0,5713
10	1,6965	0,562	1,695	0,5635
20	1,6995	0,5593	1,7065	0,5528
30	1,7263	0,5351	1,7337	0,5285
50	1,7543	0,5106	1,7609	0,5049
100	1,8093	0,4646	1,8042	0,4688
200	1,8519	0,431	1,8548	0,4287
300	1,8721	0,4155	1,8775	0,4114
500	1,8976	0,3965	1,9056	0,3906
1000	1,9377	0,3676	1,9497	0,3592
2000	1,9719	0,3439	1,9906	0,3313
2500	1,9854	0,3348	2,0047	0,3219

Table 24. 8 m Depth Disturbed Dry and Saturated Samples with 10 kPa

Applied Stress	800 cm Depth Saturated with 10kpa			
	Sample 1		Sample 2	
	Bulk Density	Void Ratio	Bulk Density	Void Ratio
[kPa]	[g/cm³]	e	[g/cm³]	e
0	1,6951	0,5633	1,7134	0,5466
10	1,714	0,5461	1,7203	0,5404
20	1,7302	0,5316	1,7268	0,5346
30	1,7444	0,5191	1,7373	0,5254
50	1,7681	0,4988	1,756	0,5091
100	1,8096	0,4644	1,7965	0,4751
200	1,8516	0,4312	1,8404	0,4399
300	1,8736	0,4144	1,8654	0,4206
500	1,8998	0,3949	1,8985	0,3958
1000	1,9329	0,371	1,9388	0,3668
2000	1,9654	0,3483	1,9797	0,3386
2500	1,9751	0,3417	1,9929	0,3297

Table 25. 8 m Depth Disturbed Dry and Saturated Samples with 20 kPa

Applied Stress	800 cm Depth Saturated with 20kpa			
	Sample 1		sample2	
	Bulk Density	Void Ratio	Bulk Density	Void Ratio
[kPa]	[g/cm³]	e	[g/cm³]	e
0	1,7402	0,5228	1,7095	0,5501
10	1,7432	0,5202	1,7095	0,5501
20	1,7564	0,5087	1,7233	0,5377
30	1,7694	0,4977	1,7364	0,5261
50	1,7908	0,4798	1,7579	0,5075
100	1,8274	0,4501	1,8052	0,468
200	1,8592	0,4254	1,8531	0,43
300	1,8772	0,4117	1,8833	0,4071
500	1,8998	0,3949	1,9224	0,3785
1000	1,9292	0,3736	1,9792	0,3389
2000	1,9597	0,3523	2,048	0,294
2500	1,9685	0,3462	2,0703	0,28

Appendix 9

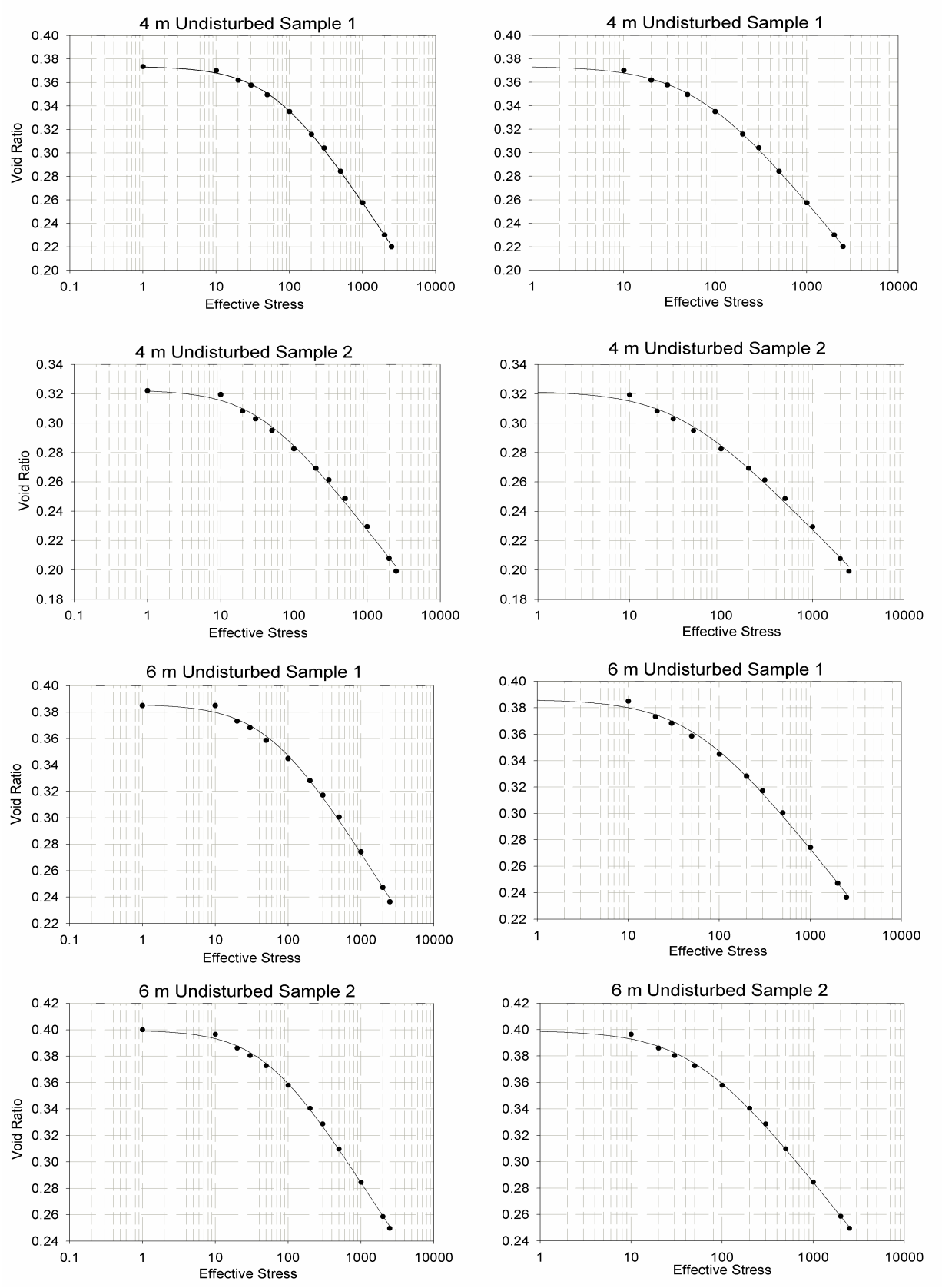

Figure 33. Undisturbed samples from 4 m and 6 m depth

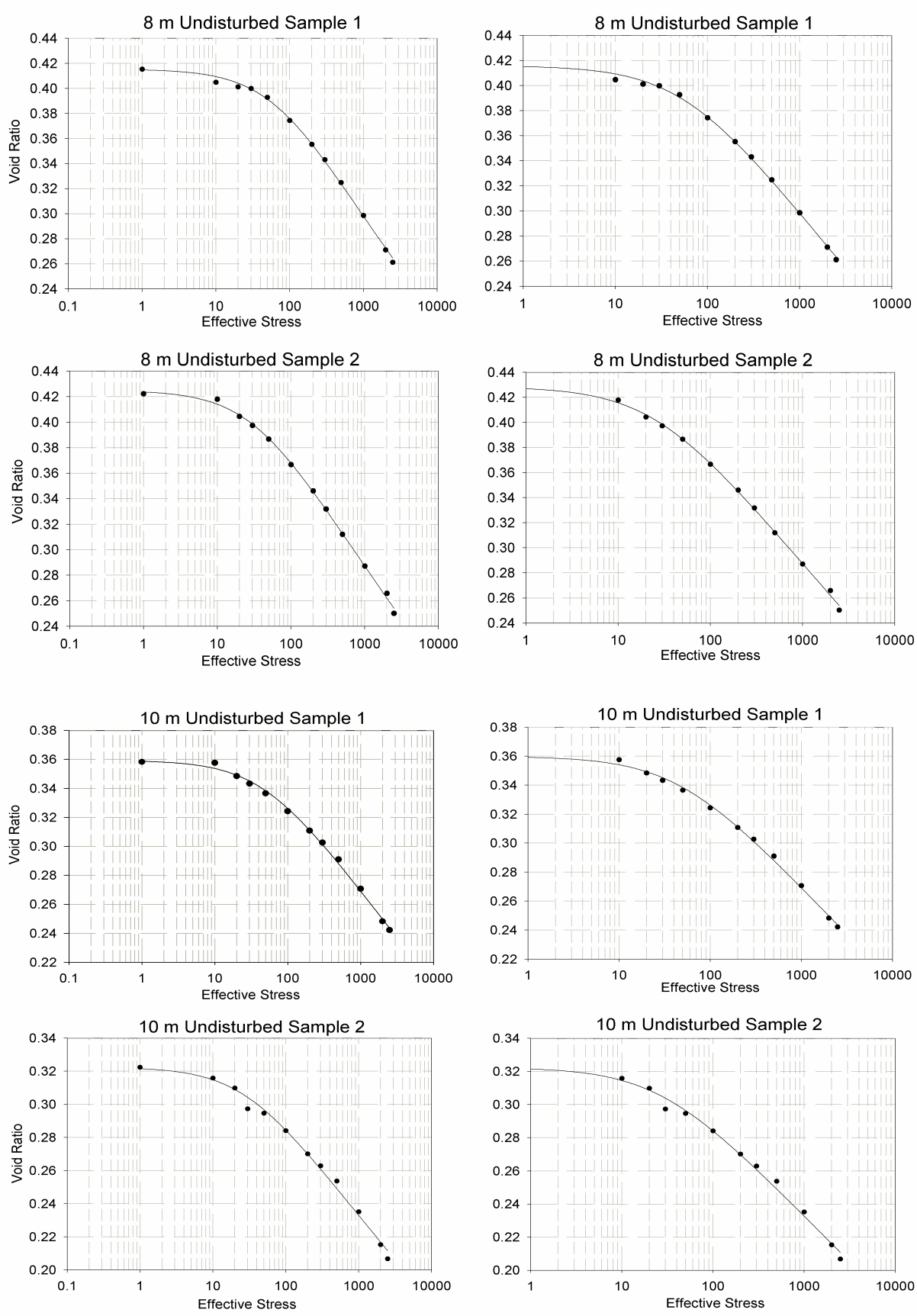

Figure 34. Undisturbed samples from 8 m and 10 m depth

Table 26. Undisturbed samples considering the void ratio value at 1 kPa

Depth	Pre-consolidation load					
	Undisturbed sample 1			Undisturbed sample 2		
	Minimum	Most Probable	Maximum	Minimum	Most Probable	Maximum
4 m	50	90	600	30	55	280
6 m	43	75	300	40	75	280
8 m	42	70	230	21	40	100
10 m	38	70	290	22	40	190

Table 27. Undisturbed samples

Depth	Pre-consolidation load					
	Undisturbed sample 1			Undisturbed sample 2		
	Minimum	Most Probable	Maximum	Minimum	Most Probable	Maximum
4 m	50	90	300	30	55	270
6 m	43	80	320	43	75	430
8 m	45	90	340	21	38	170
10 m	40	75	340	24	45	340

Table 28. Parameters used in Equation [7] to generate the consolidation curves of undisturbed samples considering 1 kPa stress

Sample depths			e_{max}	e_{min}	σ (kPa)	n	R^2
4 m with 1 kPa	Sample 1	Fitted	0.3739	-3.2308	0.0141	1.0121	0.9997
		Fixed	0.3735	-3.3401	0.0139	1.0118	0.9997
	Sample 2	Fitted	0.3226	-3.8413	0.0281	1.0069	0.9967
		Fixed	0.3221	-3.6655	0.0270	1.0072	0.9967
6 m with 1 kPa	Sample 1	Fitted	0.3860	-3.5847	0.0166	1.0101	0.9978
		Fixed	0.3849	-0.5061	0.0134	1.0503	0.9974
	Sample 2	Fitted	0.3997	-0.8905	0.0166	1.0327	0.9989
		Fixed	0.4000	-3.8391	0.0184	1.0093	0.9991
8 m with 1 kPa	Sample 1	Fitted	0.4134	-0.9329	0.0130	1.0339	0.9991
		Fixed	0.4154	-0.1404	0.0124	1.0913	0.9992
	Sample 2	Fitted	0.4249	-0.5797	0.0280	1.0437	0.9987
		Fixed	0.4222	-0.0422	0.0190	1.1150	0.9982
10 m with 1 kPa	Sample 1	Fitted	0.3593	-3.0704	0.0204	1.0087	0.9977
		Fixed	0.3583	-0.9317	0.0178	1.0244	0.9974
	Sample 2	Fitted	0.3215	-2.8850	0.0336	1.0079	0.9946
		Fixed	0.3224	-0.6286	0.0329	1.0280	0.9918

* We observed that the values of e_{min} are negative which is not possible but the curves were fitted properly with the equation used.

Table 29. Parameters used in Equation [7] to generate the consolidation curves of undisturbed samples without considering 1 kPa stress

Sample depths			e_{max}	e_{min}	σ (kPa)	n	R^2
4 m	Sample 1	Fitted	0.3737	-4.1764	0.0141	1.0095	0.9996
		Fixed	0.3735	-0.7371	0.0124	1.0425	0.9995
	Sample 2	Fitted	0.3219	-1.5683	0.0257	1.0156	0.9960
		Fixed	0.3221	-3.6805	0.0270	1.0072	0.9961
6 m	Sample 1	Fitted	0.3863	-3.6772	0.0169	1.0098	0.9976
		Fixed	0.3849	-2.6083	0.0153	1.0136	0.9974
	Sample 2	Fitted	0.3992	-1.9117	0.0170	1.0176	0.9989
		Fixed	0.4000	-3.8582	0.0184	1.0093	0.9990
8 m	Sample 1	Fitted	0.4113	-0.3293	0.0104	1.0684	0.9993
		Fixed	0.4159	-1.8622	0.0165	1.0185	0.9971
	Sample 2	Fitted	0.4284	-2.5324	0.0380	1.0133	0.9988
		Fixed	0.4222	-0.3344	0.0230	1.0620	0.9982
10 m	Sample 1	Fitted	0.3598	-3.2307	0.0213	1.0082	0.9973
		Fixed	0.3583	-0.9343	0.0178	1.0244	0.9970
	Sample 2	Fitted	0.3186	-2.3983	0.0262	1.0097	0.9933
		Fixed	0.3224	-3.1400	0.0363	1.0073	0.9928

Appendix 10

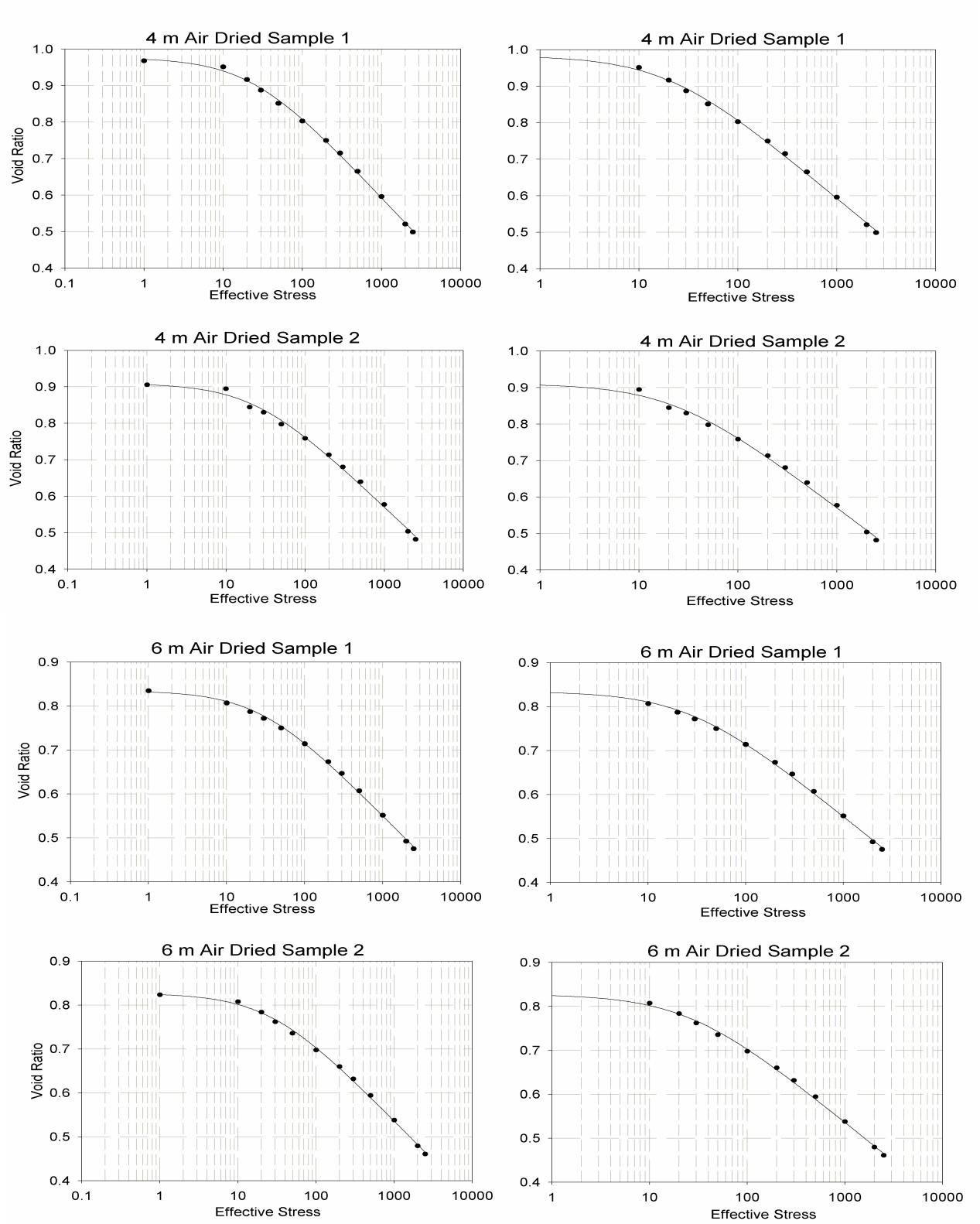

Figure 35. Disturbed dry sample from 4 m and 6 m depth

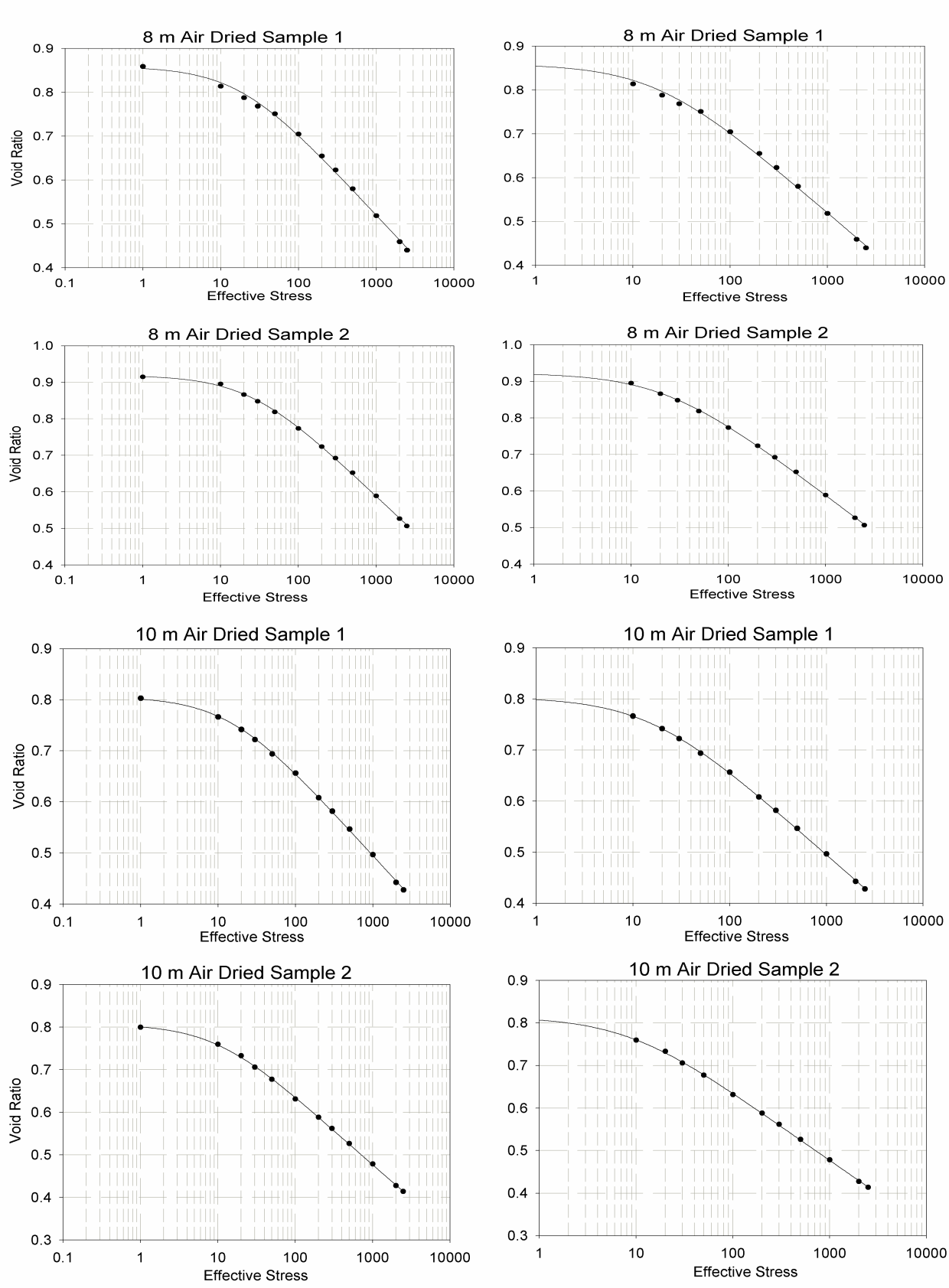

Figure 36. Disturbed dry samples from 8 m and 10 m depth

Table 30. Disturbed dry samples considering the void ratio value at 1 kPa

Depth	Pre-consolidation load					
	Air Dried sample 1			Air Dried sample 2		
	Minimum	Most Probable	Maximum	Minimum	Most Probable	Maximum
4 m	20	36	190	21	38	210
6 m	22	41	190	23	40	180
8 m	18	30	160	20	35	180
10 m	12	22	100	9	18	65

Table 31. Disturbed dry samples

Depth	Pre-consolidation load					
	Air Dried sample 1			Air Dried sample 2		
	Minimum	Most Probable	Maximum	Minimum	Most Probable	Maximum
4 m	19	35	160	21	40	205
6 m	28	50	250	21	35	160
8 m	18	35	180	20	35	180
10 m	14	25	170	8	15	70

Table 32. Parameters used in Equation [7] to generate the consolidation curves of disturbed dry samples considering 1 kPa stress

Sample depths			e_{max}	e_{min}	σ (kPa)	n	R^2
4 m	Sample 1	Fitted	0.9761	-10.7818	0.0410	1.0089	0.9987
		Fixed	0.9680	-5.0644	0.0339	1.0181	0.9984
	Sample 2	Fitted	0.9092	-12.4600	0.0400	1.0069	0.9965
		Fixed	0.9051	-7.7324	0.0359	1.0109	0.9963
6 m	Sample 1	Fitted	0.8299	-5.4349	0.0297	1.0134	0.9988
		Fixed	0.8343	-6.7682	0.0338	1.0108	0.9987
	Sample 2	Fitted	0.8263	-7.6785	0.0357	1.0096	0.9986
		Fixed	0.8229	-1.5999	0.0291	1.0371	0.9983
8 m	Sample 1	Fitted	0.8528	-6.1719	0.0455	1.0127	0.9984
		Fixed	0.8586	-7.8175	0.0525	1.0100	0.9982
	Sample 2	Fitted	0.9189	-4.5840	0.0365	1.0171	0.9996
		Fixed	0.9143	-5.5746	0.0335	1.0146	0.9995
10 m	Sample 1	Fitted	0.8058	-7.4243	0.0667	1.0091	0.9997
		Fixed	0.8030	-1.9195	0.0560	1.0297	0.9999
	Sample 2	Fitted	0.8071	-2.7602	0.0900	1.0297	0.9999
		Fixed	0.7993	-1.0008	0.0668	1.0469	0.9994

Table 33. Parameters used in Equation [7] to generate the consolidation curves of disturbed dry samples without considering 1 kPa stress

Sample depths			e_{max}	e_{min}	σ (kPa)	n	R^2
4 m	Sample 1	Fitted	0.9831	-6.0850	0.0452	1.0148	0.9985
		Fixed	0.9680	-5.1336	0.0340	1.0179	0.9981
	Sample 2	Fitted	0.9102	-12.3104	0.0408	1.0070	0.9958
		Fixed	0.9051	-7.7848	0.0359	1.0109	0.9956
6 m	Sample 1	Fitted	0.8208	-7.5240	0.0240	1.0103	0.9994
		Fixed	0.8343	-6.8118	0.0338	1.0107	0.9985
	Sample 2	Fitted	0.8273	-7.9713	0.0366	1.0093	0.9984
		Fixed	0.8229	-1.6090	0.0291	1.0369	0.9980
8 m	Sample 1	Fitted	0.8326	-2.5161	0.0274	1.0294	0.9994
		Fixed	0.8586	-7.9195	0.0526	1.0099	0.9979
	Sample 2	Fitted	0.9225	-17.7983	0.0417	1.0048	0.9996
		Fixed	0.9143	-4.5092	0.0331	1.0176	0.9994
10 m	Sample 1	Fitted	0.7988	-4.5002	0.0553	1.0147	0.9998
		Fixed	0.8030	-13.5062	0.0640	1.0052	0.9998
	Sample 2	Fitted	0.8140	-3.2534	0.1051	1.0185	0.9997
		Fixed	0.7993	-1.2026	0.0690	1.0414	0.9995

Appendix 11

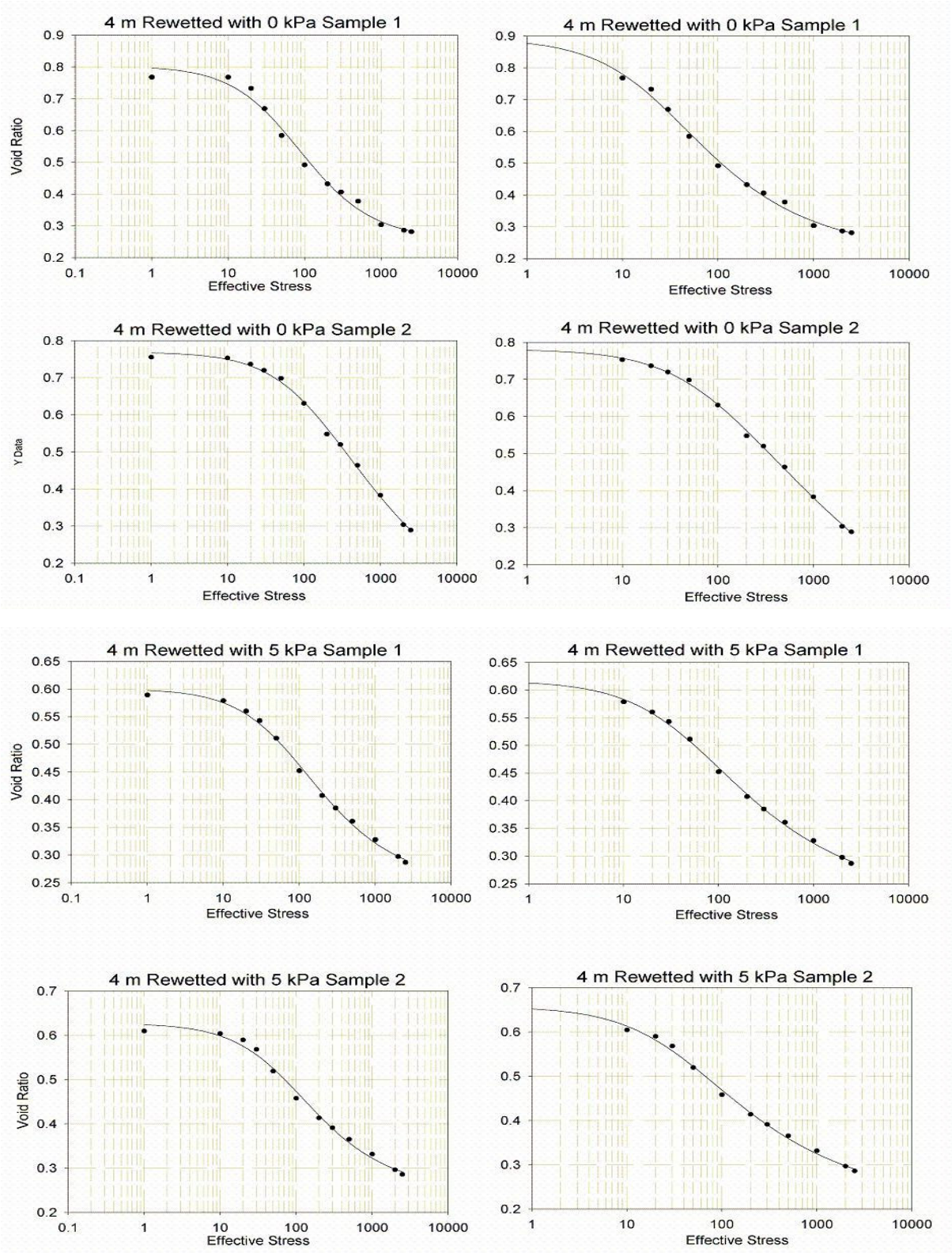

Figure 37. 4 m depth disturbed saturated curves with 0 kPa and 5 kPa pre-loads

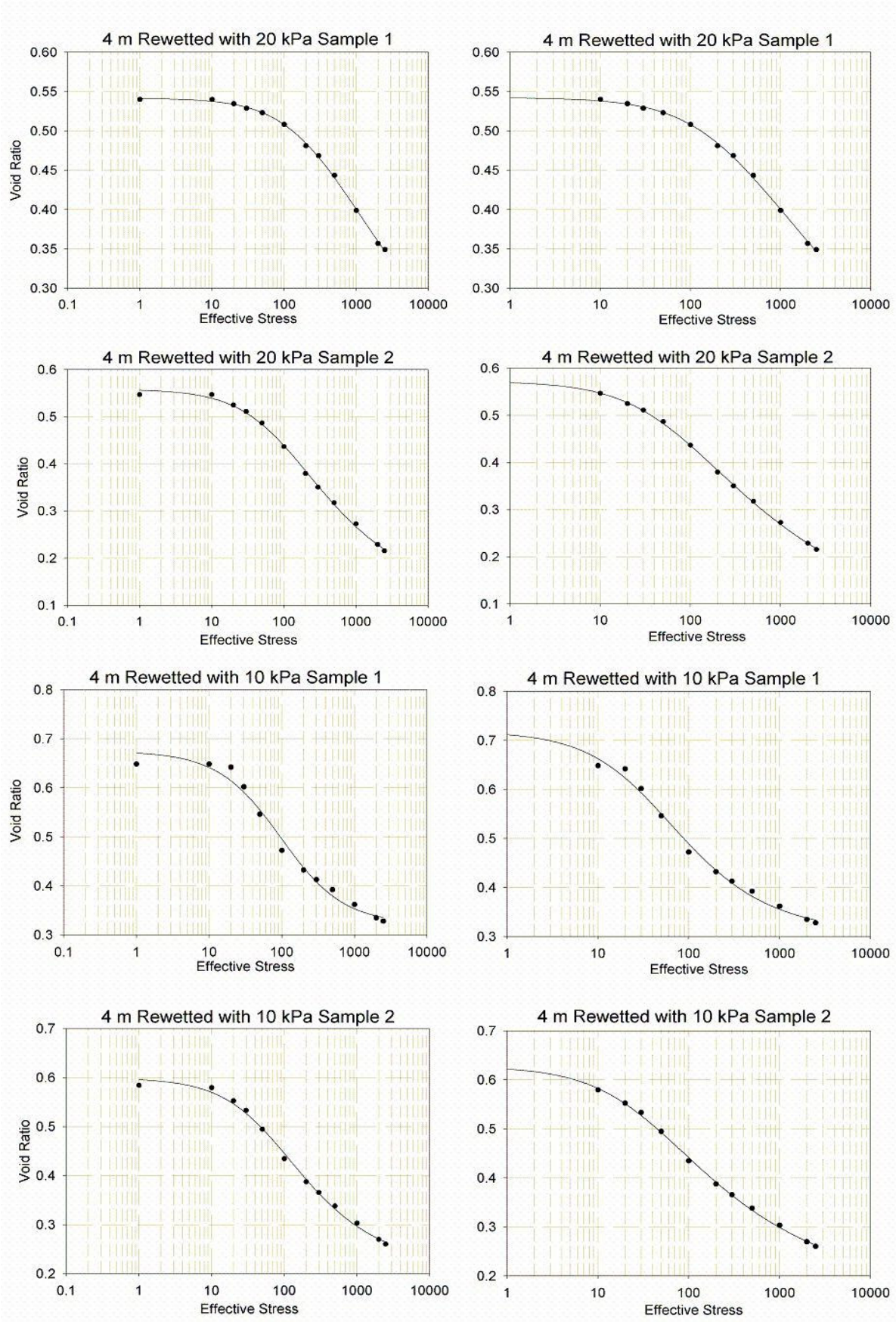

Figure 38. 4 m depth disturbed saturated curves with 10 kPa and 20 kPa pre-loads

Table 34. 4 m Depth disturbed dry and saturated samples considering void ratio value at 1 kPa

Depth 4 m with stress	Pre-consolidation load					
	Rewetted sample 1			Rewetted sample 2		
	Minimum	Most Probable	Maximum	Minimum	Most Probable	Maximum
0 kPa	11	18	50	35	55	140
5 kPa	16	22	60	14	22	60
10 kPa	19	20	65	14	20	58
20 kPa	90	150	400	21	35	90

Table 35. 4 m Depth disturbed dry and saturated samples

Depth 4 m with stress	Pre-consolidation load					
	Rewetted sample 1			Rewetted sample 2		
	Minimum	Most Probable	Maximum	Minimum	Most Probable	Maximum
0 kPa	11	10	50	30	50	180
5 kPa	11	18	41	9	12	32
10 kPa	20	11	70	17	12	65
20 kPa	90	150	400	18	30	90

Table 36. Parameters used in Equation [7] to generate the consolidation curves of disturbed dry and saturated samples from 4 m depth considering 1 kPa stress

Stress			e_{max}	e_{min}	σ (kPa)	n	R^2
0 kPa	Sample 1	Fitted	0.8028	0.2546	0.0147	1.8109	0.9886
		Fixed	0.7674	0.2667	0.0085	2.0735	0.9837
	Sample 2	Fitted	0.7687	-0.0283	0.0086	1.2970	0.9981
		Fixed	0.7554	0.1044	0.0053	1.4760	0.9970
5 kPa	Sample 1	Fitted	0.6003	0.2442	0.0137	1.5672	0.9973
		Fixed	0.5894	0.2584	0.0094	1.7148	0.9960
	Sample 2	Fitted	0.6271	0.2471	0.0137	1.6008	0.9935
		Fixed	0.6095	0.2632	0.0082	1.8029	0.9903
10 kPa	Sample 1	Fitted	0.6742	0.3227	0.0101	2.0139	0.9862
		Fixed	0.6485	0.3194	0.0074	2.0275	0.9779
	Sample 2	Fitted	0.5988	0.2107	0.0154	1.5379	0.9966
		Fixed	0.5480	0.2289	0.0098	1.7050	0.9945
20 kPa	Sample 1	Fitted	0.5416	0.0339	0.0040	1.2013	0.9991
		Fixed	0.5399	0.1802	0.0028	1.3677	0.9990
	Sample 2	Fitted	0.5578	0.1121	0.0104	1.4346	0.9984
		Fixed	0.5466	0.1519	0.0065	1.6203	0.9970

Table 37. Parameters used in Equation [7] to generate the consolidation curves of disturbed dry and saturated samples from 4 m depth without considering 1 kPa stress

stress			e_{max}	e_{min}	σ (kPa)	n	R^2
0 kPa	Sample 1	Fitted	0.8911	0.2150	0.0433	1.4983	0.9944
		Fixed	0.7674	0.2667	0.0085	2.0716	0.9800
	Sample 2	Fitted	0.7806	-0.2563	0.0133	1.1832	0.9987
		Fixed	0.7554	0.1042	0.0053	1.4755	0.9966
5 kPa	Sample 1	Fitted	0.6164	0.2176	0.0230	1.4183	0.9983
		Fixed	0.5894	0.2583	0.0094	1.7135	0.9952
	Sample 2	Fitted	0.6571	0.2088	0.0297	1.3945	0.9963
		Fixed	0.6095	0.2631	0.0083	1.8017	0.9884
10 kPa	Sample 1	Fitted	0.7181	0.3057	0.0246	1.6520	0.9921
		Fixed	0.6485	0.3293	0.0054	2.4299	0.9755
	Sample 2	Fitted	0.6271	0.1641	0.0336	1.3483	0.9989
		Fixed	0.5840	0.2287	0.0098	1.7037	0.9934
20 kPa	Sample 1	Fitted	0.5422	0.0165	0.0042	1.1900	0.9990
		Fixed	0.5399	0.1800	0.0028	1.3674	0.9989
	Sample 2	Fitted	0.5716	0.0344	0.0182	1.2805	0.9995
		Fixed	0.5466	0.1514	0.0065	1.6174	0.9966

Appendix 12

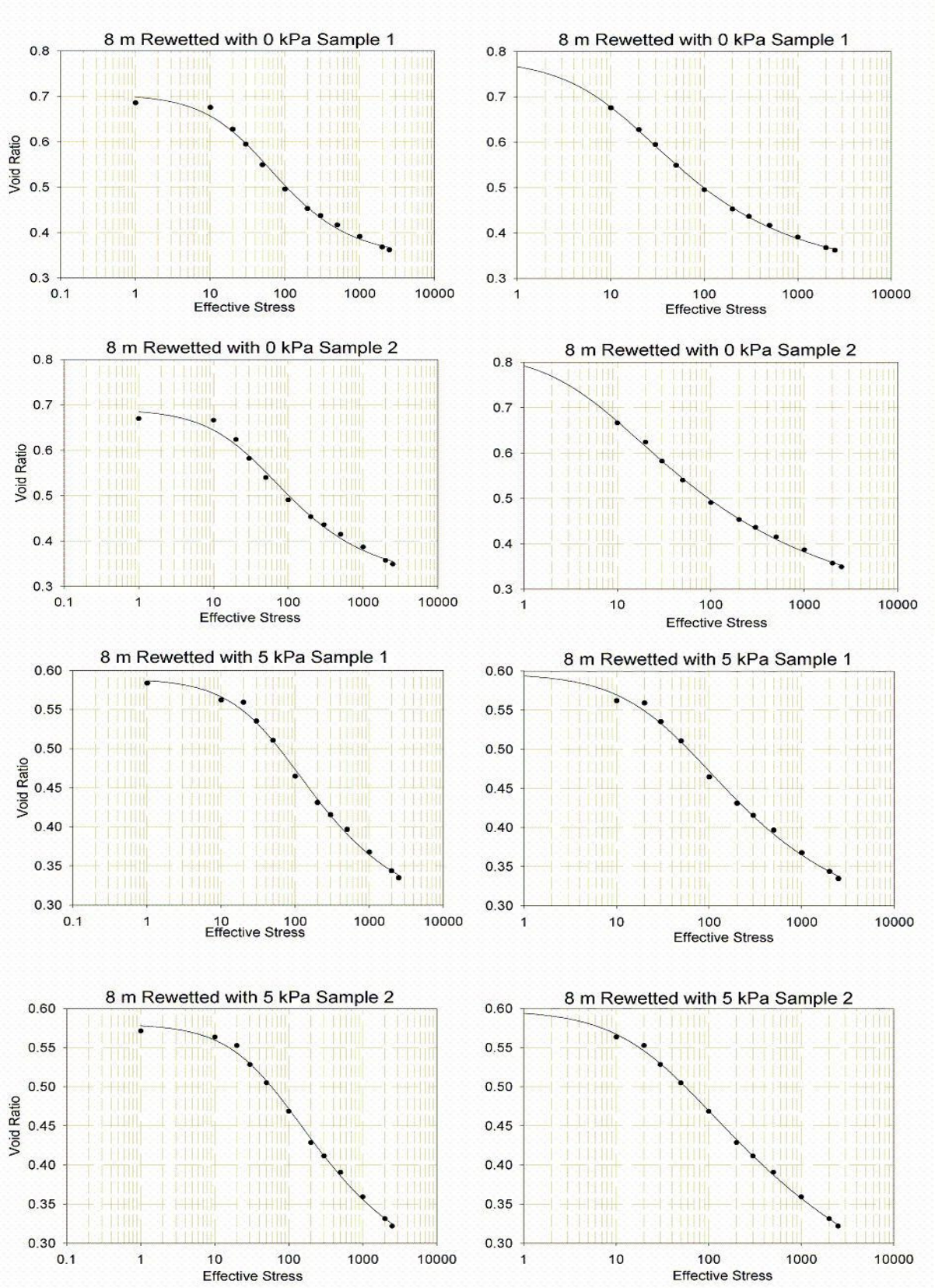

Figure 39. 8 m depth disturbed saturated curves with 0 kPa and 5 kPa pre-loads

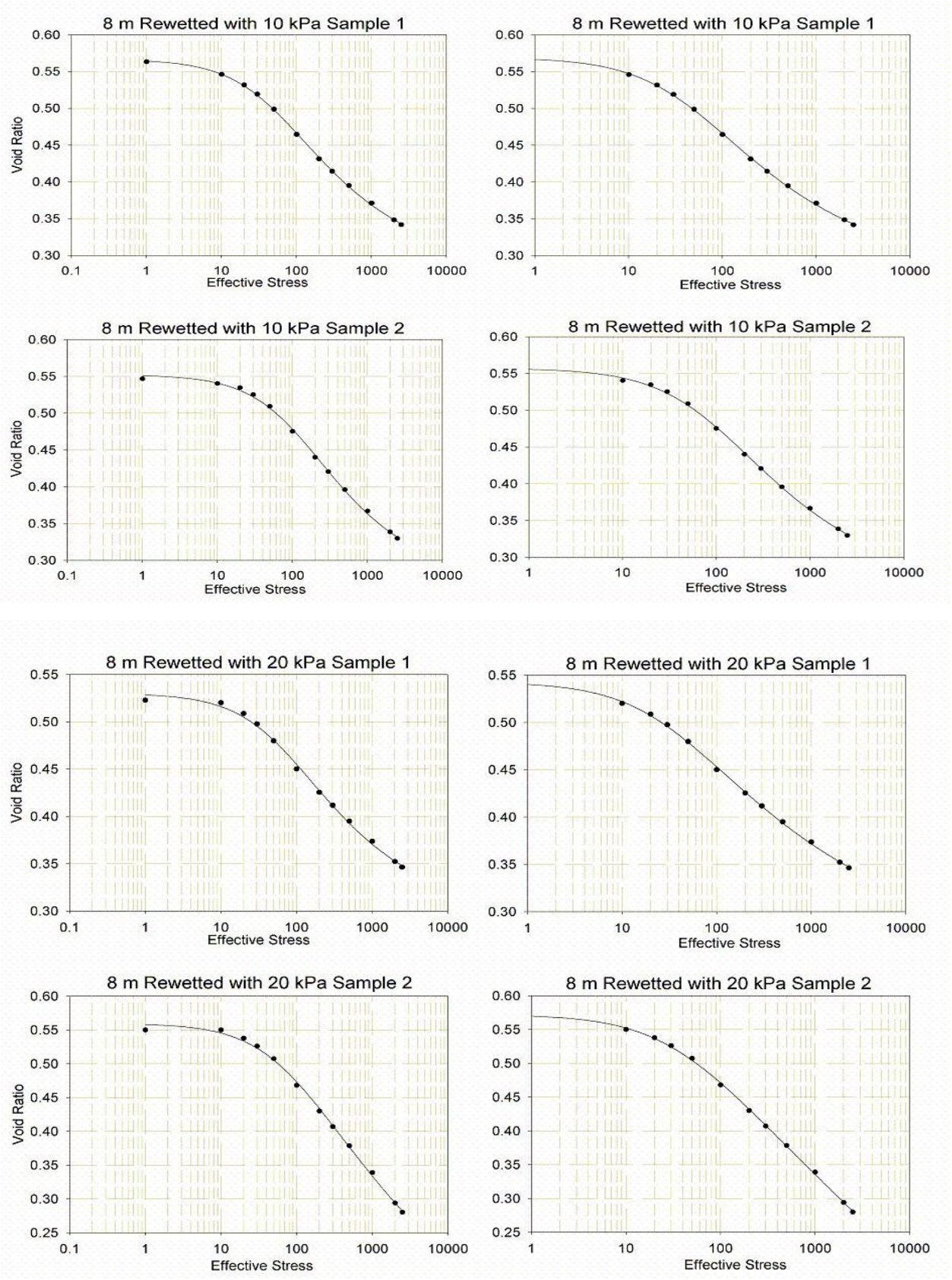

Figure 40. 8 m depth disturbed saturated curves with 10 kPa and 20 kPa pre-loads

Table 38. 8 m Depth disturbed dry and saturated samples considering void ratio value at 1 kPa

Depth 8 m with stress	Pre-consolidation load					
	Rewetted sample 1			Rewetted sample 2		
	Minimum	Most Probable	Maximum	Minimum	Most Probable	Maximum
0 kPa	8	12	34	8	12	38
5 kPa	11	19	48	12	21	55
10 kPa	11	20	55	25	40	100
20 kPa	16	25	58	25	40	110

Table 39. 8 m Depth disturbed dry and saturated samples

Depth 8 m with stress	Pre-consolidation load					
	Rewetted sample 1			Rewetted sample 2		
	Minimum	Most Probable	Maximum	Minimum	Most Probable	Maximum
0 kPa	4	6	18	2	3	9
5 kPa	11	19	43	10	17	36
10 kPa	11	20	54	21	35	90
20 kPa	10	18	41	19	30	80

Table 40. Parameters used in Equation [7] to generate the consolidation curves of disturbed dry and saturated samples from 8 m depth considering 1 kPa stress

stress			e_{max}	e_{min}	σ (kPa)	n	R^2
0 kPa	Sample 1	Fitted	0.7039	0.3447	0.0229	1.6855	0.9945
		Fixed	0.6857	0.3519	0.0152	1.8335	0.9918
	Sample 2	Fitted	0.6902	0.3141	0.0286	1.5164	0.9910
		Fixed	0.6696	0.3256	0.0181	1.6345	0.9874
5 kPa	Sample 1	Fitted	0.5895	0.2835	0.0197	1.4390	0.9985
		Fixed	0.5838	0.2937	0.0155	1.5062	0.9960
	Sample 2	Fitted	0.5803	0.2438	0.0186	1.3690	0.9975
		Fixed	0.5713	0.2682	0.0124	1.4824	0.9961
10 kPa	Sample 1	Fitted	0.5665	0.2776	0.0215	1.3709	0.9997
		Fixed	0.5633	0.2872	0.0181	1.4154	0.9995
	Sample 2	Fitted	0.5520	0.2701	0.0086	1.4889	0.9988
		Fixed	0.5466	0.2894	0.0059	1.6502	0.9980
20 kPa	Sample 1	Fitted	0.5298	0.2912	0.0166	1.3833	0.9976
		Fixed	0.5228	0.3102	0.0105	1.5205	0.9959
	Sample 2	Fitted	0.5595	-0.0215	0.0145	1.1792	0.9982
		Fixed	0.5501	7.7590	0.0213	0.9907	0.9944

Table 41. Parameters used in Equation [7] to generate the consolidation curves of disturbed dry and saturated samples from 8 m depth without considering 1 kPa stress

stress			e_{max}	e_{min}	σ (kPa)	n	R^2
0 kPa	Sample 1	Fitted	0.7815	0.3113	0.0847	1.4083	0.9993
		Fixed	0.6857	0.3518	0.0153	1.8304	0.9895
	Sample 2	Fitted	0.8211	0.2439	0.2141	1.2661	0.9982
		Fixed	0.6696	0.3254	0.0182	1.6322	0.9841
5 kPa	Sample 1	Fitted	0.5968	0.2694	0.0262	1.3729	0.9961
		Fixed	0.5838	0.2934	0.0156	1.5046	0.9951
	Sample 2	Fitted	0.5976	0.1796	0.0380	1.2334	0.9987
		Fixed	0.5713	0.2680	0.0124	1.4813	0.9954
10 kPa	Sample 1	Fitted	0.5691	0.2699	0.0245	1.3415	0.9997
		Fixed	0.5633	0.2868	0.0182	1.4137	0.9994
	Sample 2	Fitted	0.5570	0.2464	0.0119	1.3788	0.9993
		Fixed	0.5466	0.2893	0.0059	1.6494	0.9977
20 kPa	Sample 1	Fitted	0.5426	0.2408	0.0355	1.2320	0.9993
		Fixed	0.5228	0.3101	0.0105	1.5195	0.9952
	Sample 2	Fitted	0.5720	-0.6346	0.0292	1.0640	0.9995
		Fixed	0.5501	0.1209	0.0084	1.3150	0.9963